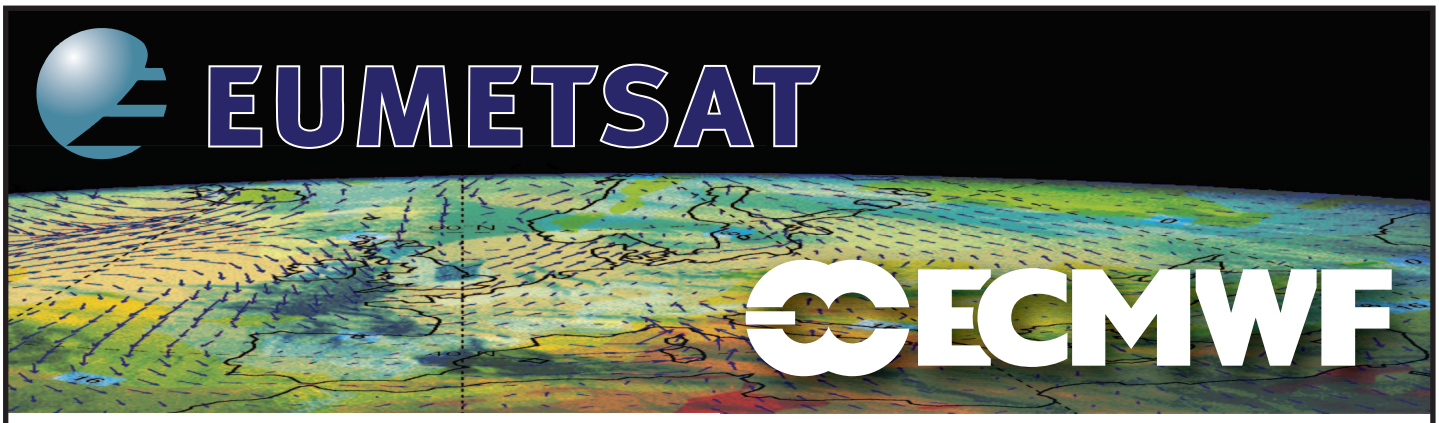

EUMETSAT/ECMWF Fellowship Programme
Research Report No. 34

First year report: The impact of HIRS on ECMWF forecasts, adding ATMS data over land and sea-ice and new observation errors for AMSU-A

Heather Lawrence and Niels Bormann

October 2014

Series: EUMETSAT/ECMWF Fellowship Programme Research Reports

A full list of ECMWF Publications can be found on our web site under:
http://www.ecmwf.int/publications/

Contact: library@ecmwf.int

European Centre for Medium Range Weather Forecasts
Shinfield Park, Reading, RG2 9AX, England

1 Executive Summary

Clear-sky observations from Microwave (MW) and Infra-Red (IR) sounders are currently assimilated directly as radiances into the ECMWF assimilation system, where they have a significant impact on atmospheric temperature, humidity and wind fields. The microwave sounders include the AMSU-A temperature sounders, MHS humidity sounders and the newer ATMS instrument which combines both temperature and humidity sounding channels. The infra-red instruments include the older HIRS instrument and the newer hyperspectral IASI and AIRS sounders, all of which have temperature and water vapour sounding channels, as well as some channels which contain information on ozone. AMSU-A, MHS and HIRS together make up the ATOVS suite of instruments. The purpose of this fellowship is to improve the usage of ATOVS instruments and ATOVS-like instruments such as ATMS in the ECMWF forecasting system.

In the first year of this fellowship, three different studies were carried out. The first study was to assess the impact of the HIRS instrument in the ECMWF system. This was done for two reasons. Firstly the operational 4DVAR system has gone through many upgrades since HIRS radiances were first assimilated at ECMWF and the effect of HIRS data on the system has not been verified in recent years. Secondly HIRS provides similar information to IASI and AIRS and at similar orbit times but with a lower vertical resolution. It is therefore of interest to investigate whether the HIRS radiances are still having an effect. The assessment was done by performing simulations of the ECMWF forecasting system without the HIRS data and comparing the results to the operational setup. We found that including HIRS improved the fit of the 12-hour forecast to the humidity sounder MHS by 0.5 % and IR temperature sounders IASI and AIRS by 0.5 - 1 % and produced a 0.5 % improvement in the short-range forecasts for temperature and geopotential in the Southern Hemisphere. These changes, although small were found to be statistically significant, indicating an improvement in short-range temperature and humidity forecasts when HIRS is actively assimilated.

The second study was to test extending the coverage of the ATMS instrument over land and sea-ice. ATMS is one of the newest sounding instruments to be assimilated at ECMWF: it was launched on NASA's Suomi-NPP satellite in 2011, and has been assimilated operationally at ECMWF since 26 September 2012. The initial operational setup included all temperature and humidity sounding channels over ocean and only the higher peaking, non-surface sensitive, temperature sounding channels over land and sea-ice. This setup was shown to have a small positive impact on forecast scores ([2]), which motivated us to try extending the global coverage of ATMS by assimilating all channels over land and sea-ice. Assimilation trials were carried out and these indicated that introducing ATMS data over land had a positive impact on temperature and humidity forecasts. However some mixed results were obtained when introducing ATMS data over sea-ice: the fit of 12-hour forecasts to the MHS instrument improved but a slight negative impact on temperature forecasts over the southern Hemisphere ocean was observed. It was therefore decided to introduce ATMS data over land into the operational system (cycle 40R3 September 2014) but not over sea-ice, pending further tests.

The third study was to develop and test situation-dependent observation errors for clear-sky assimilation of the surface-sensitive channels of AMSU-A, which includes channels 5 - 7 (frequencies of 52.8 GHz, 53.596 $\pm$ 0.115 GHz, and 54.4 GHz). Currently a single value is used for the observation errors of each channel. In this study we developed observation errors which took into account uncertainties in the surface emissivity and errors due to the presence of undetected cloud. These errors included terms

depending on the surface-to-space transmittance, skin temperature and atmospheric liquid water path. The study follows on from the work of [8] with the added development of the cloud term. We tested the new observation errors in assimilation trials. Firstly we ran trials introducing these new terms with the current operational setup. Secondly we ran simulations where the screening was to some extent relaxed over high orography and in cloudy conditions, allowing in more data but with higher observation errors so that it has less weight in the analysis. Results indicated that the new observation errors without changing the screening (i.e. with the same number of data) had a neutral impact on forecast scores. However some positive impacts were observed on the 12-hour fit to ATMS observations and in forecast scores of geopotential height when the cloud-screening was relaxed. This study is still ongoing and further tests will be made in the future.

2 HIRS: Testing the impact on the ECMWF Numerical Weather Prediction Model

2.1 Introduction

The HIRS instrument is an infra-red sounder with CO_2, CO_2/N_2O and water vapour channels. The former two provide information on atmospheric temperature at different levels of the atmosphere and the latter includes two channels which provide information on the atmospheric humidity, with peak sensitivities at 500hPa and 700hPa. At the time of this study HIRS data were actively assimilated for the instruments aboard the NOAA-19 and MetOp-A satellites, which orbit the Earth at a local time of 9:30 and 13:37 respectively for the ascending orbit. Due to a recent increase in the instrument noise, the NOAA-19 HIRS data is no longer actively assimilated. Note that tests are ongoing for the possible introduction of MetOp-B HIRS.

In order to investigate the impact of HIRS data, assimilation trials were performed in which the HIRS radiances were no longer assimilated and the effect on the forecast scores and departure statistics was assessed. These assimilation experiments are described in section 2.2 and the results are discussed in section 2.3.

2.2 Assimilation experiment setup

Four different assimilation experiments were carried out. Firstly experiments actively assimilating HIRS radiances were run for two seasons: 1 January - 29 February 2012 and 1 July - 31 August 2012. These two experiments were considered to be the control experiments. Secondly two experiments where the HIRS radiances were not actively assimilated were run over the same periods. Hereafter we will refer to these experiments as the 'No Hirs' experiments. All experiments used Cycle 38r2 of the assimilation system and had a spatial resolution of T511 ($\sim$40 km), an incremental analysis resolution of T255 ($\sim$80 km) and 137 levels in the vertical. 10 day forecasts were calculated from each 0z analysis. The departure statistics and forecast scores for all four experiments were compared to each other in order to assess the influence of the HIRS radiances.

2.3 Results

2.3.1 First Guess Departure Statistics

One way of assessing the impact of the HIRS radiances on the NWP system is to look at statistics for the observations minus the background, known as the background or First Guess (FG) departure statistics. This allows us to compare 12 hour forecasts to observations, which include conventional data such as radiosondes, as well as satellite data. We are particularly interested in the impact of HIRS assimilation on the humidity and temperature profiles provided by radiosondes at heights of of 200 - 1000 hPa, since the HIRS IR channels are most sensitive to this, and also the departure statistics of other satellite instruments whose measurements are also sensitive to humidity and temperature. These latter satellites include CrIS, AIRS, and IASI IR sounders and MHS which is a microwave humidity sounder.

FG-departure statistics for radiosonde measurements of wind vectors, temperature and humidity were calculated and there were found to be some changes for the temperature radiosondes when HIRS radiances were assimilated, which are shown in figure 1. This figure indicates an improvement of fits to temperature radiosondes at 500hPa and a degradation at 1000hPa in the Northern Hemisphere extra-tropics. The improvement was seen in both the summer and winter experiments but the degradation was seen only in the Northern Hemisphere summer experiment. There were no significant differences in humidity radiosonde departures but some slight reductions in the standard deviation of background departures for vector wind radiosondes over the Northern Hemisphere.

There are slight improvements in the departure statistics of the MHS radiances over all three assimilated channels; standard deviations of MHS background departures were reduced by approximately 0.4% when HIRS was assimilated, as shown in figure 2, and this was consistent for the Northern Hemisphere extra-tropics, Southern Hemisphere extra-tropics and tropics as well as for the MHS instruments on the different satellites (NOAA-18, NOAA-19, MetOp-A). There were also generally lower biases between MHS observations and the background when HIRS was assimilated. The assimilation of HIRS radiances also reduced the standard deviation of background departures for the water vapour and ozone channels of AIRS and IASI (shown in figure 2) by up to 1 % as well as SSMI/S by 0.1 - 0.2 %, especially the humidity-sensitive channels. These reductions were found to be statistically significant in the 95th percentile. The reduction in the departure statistics for these instruments indicates that the HIRS radiance assimilation improves short-range forecasts, particularly of humidity, since it brings the radiances simulated from these 12 hour forecasts closer to observations.

2.3.2 Forecast scores

When assessing the impact of a change in the data assimilation system we would like to study the effect on the forecast accuracy, which can be done by looking at the changes in forecast scores. Forecast scores are the root mean square difference between forecast and analysis, averaged over time for each forecast step (12 hour - 10 days). In this case we assume that the analysis is a close representation of the true value.

Temperature, geopotential, humidity and vector wind forecast scores were calculated for each experiment over each season, and then the difference between the 'No HIRS' experiments and the control was calculated in order to assess the impact of HIRS. These were normalised to the control experiments and values were averaged over the Northern Hemisphere extra tropics, Southern Hemisphere extra tropics, and tropics, at levels of 1000, 850, 700, 500, 200, 100, and 50 hPa. Results showed that overall the assimilation of HIRS radiances produced a neutral to slightly positive impact on the forecasts for geopo-

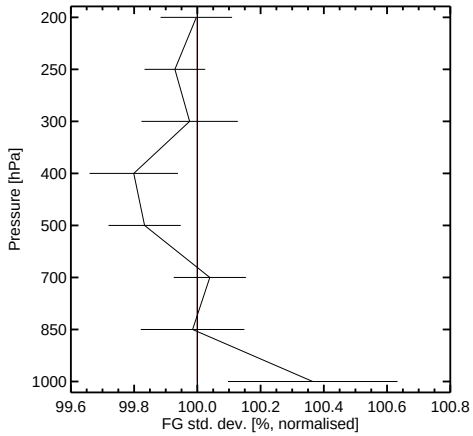

Figure 1: Standard deviation of (o-b) of the for the AIREP Temperature radiosondes as a function of atmospheric height in hPa for the 'No HIRS' experiments normalised to the control. Values are averaged over the Northern Hemisphere extra-tropics and for 4 months of experimentation including both the winter and summer periods. Values below 100% indicate a reduction in standard deviation of background departures when HIRS data is used.

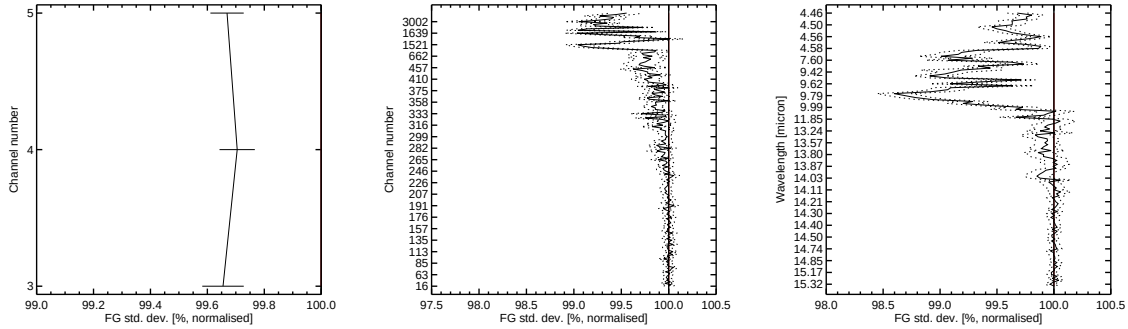

Figure 2: Difference in departure statistics of the MHS, IASI and AIRS instruments (left-to right) as a function of channel number (y axis) for the 'No HIRS' experiments, normalised to the departure statistics of the control. Values are averaged globally and over 4 months of experimentation including both the winter and summer periods. Values below 100% indicate a reduction in standard deviation of background departures when HIRS data is used.

tential, temperature and wind vector. To illustrate this, figure 3 shows these forecast scores at 500hPa for the Southern Hemisphere extra-tropics as a function of forecast day. Values are averaged over both seasons and compared to own analyses. Slightly positive impacts (about 0.5 % improvement) were observed for the Southern Hemisphere 0 - 3 day geopotential forecasts which is also shown as a function of latitude and pressure in figure 4. The impact on temperature and wind was mostly neutral to slightly positive. Forecast scores of humidity were mainly neutral but with a slight negative impact in days 1 - 2, as shown in figure 3. This was not observed in the humidity forecast scores verified against the operational analysis, indicating that this is likely to be due more to an increased variation in the analysis rather than a degradation in the accuracy of the forecasts. Furthermore, there was an improvement in the departure statistics of MHS and other humidity-sensitive observations, as shown in Figure 2, indicating an improvement in the fit of humidity-dependent observations to 12-hour forecasts.

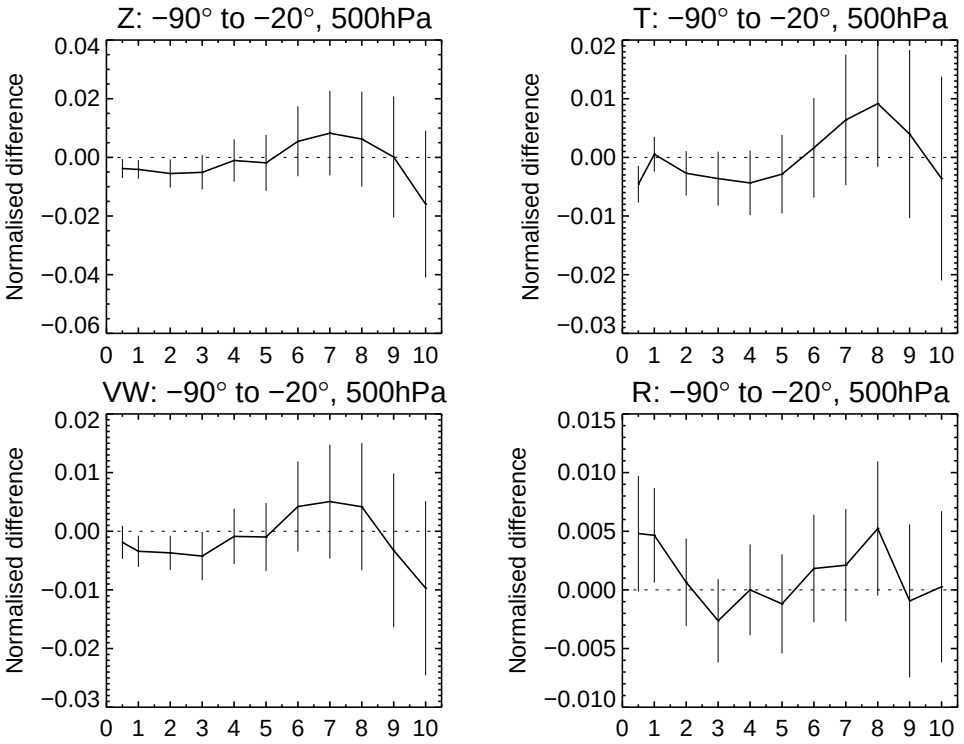

Figure 3: Normalised difference in the root mean square forecast error as a function of forecast day for the Southern Hemisphere extra tropics at 500 hPa for (left-to-right and top-to-bottom) geopotential, temperature, vector wind and humidity. Values show forecast scores verified against own analysis for the control minus 'No HIRS' experiments and are averaged over both seasons. Negative values indicate that HIRS radiances have a positive impact on forecast scores.

2.4 Conclusions

In this section we investigated the impact of HIRS radiances on the ECMWF data assimilation system. Four assimilation experiments were performed over two seasons: January - February 2012 and July - August 2012. For each season a control experiment was performed where HIRS was actively assimilated (as with the operational system) and a 'No HIRS' experiment was performed where HIRS radiances were not actively assimilated. Background departure statistics and forecast scores were compared for the control and 'no HIRS' experiments. These statistics showed an improved fit of observations to 12-hour forecasts (background) for the MHS, IASI and AIRS instruments. Forecast scores indicated an overall

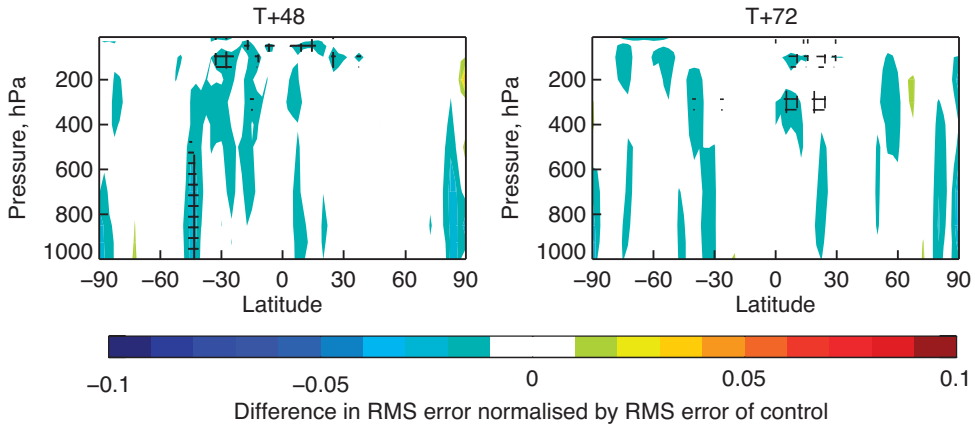

Figure 4: Normalised difference in the root mean square geopotential forecast error as a function of latitude (x-axis) and pressure (y-axis) for day 2 forecasts (left) and day 3 forecasts (right).Forecasts are verified against own analysis and averaged over both seasons. Negative (blue) values indicate that HIRS radiances have a positive impact on forecast scores and the bars indicate that this is statistically significant.

neutral to slightly positive impact for the assimilation of HIRS radiances for temperature, geopotential and wind vector. We conclude that HIRS has a neutral to positive impact on assimilation and forecasts.

3 ATMS

3.1 Introduction

The ATMS instrument is flown aboard NASA's Suomi-NPP satellite, launched in 2011. This instrument combines heritage channels for temperature and humidity sounding from AMSU-A and MHS respectively with two new humidity sounding channels and an additional window channel. The weighting functions for the different sounding channels are shown in figure 5. ATMS data are sampled more densely than AMSU-A with a smaller footprint and a larger noise. Before assimilation the ATMS data are averaged over 3 neighbouring scan positions and 3 scan lines to reduce the noise to desirable levels [2]. After this 3 x 3 averaging, ATMS has lower noise levels than equivalent channels on AMSU-A and MHS instruments flown aboard the NOAA and MetOp satellite series. However a cross-track striping pattern was observed in first guess departures indicating a scanline-dependent correlated error. Furthermore [2] found a higher interchannel error correlation for ATMS than for AMSU-A. Because of this, the ATMS data is assigned a higher observation error than AMSU-A and MHS in the ECMWF 4D-VAR assimilation system, and thus given less weight than AMSU-A or MHS in the assimilation. Assimilation trials indicated that introducing ATMS in this manner produced an improvement in tropospheric humidity and temperature fields (see [2]).

Currently all sounding channels are assimilated over ocean and only channels 10 - 15, the stratospheric and lower tropospheric temperature channels, are assimilated over land and sea-ice. Here we present results of studies to extend the ATMS coverage over land and sea-ice for the additional surface-sensitive channels. To do this we follow methods developed for the assimilation of AMSU-A and MHS over land and sea-ice ([6], [8], [7]), which are described in 3.2.

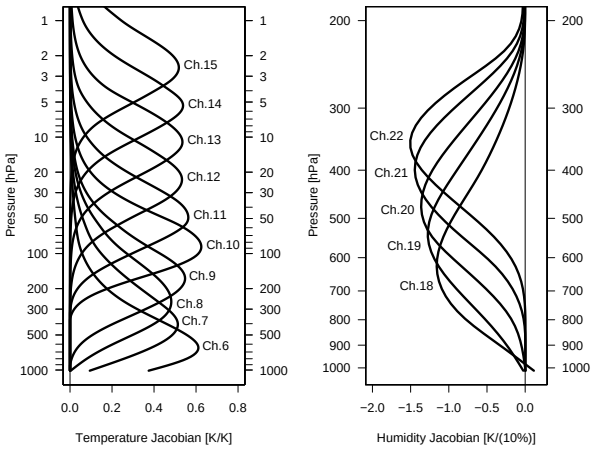

Figure 5: ATMS weighting functions at nadir for left) temperature sounding channels and right) humidity sounding channels

3.2 Method for the Assimilation of surface-sensitive ATMS channels over land and sea-ice

For the assimilation of surface-sensitive temperature and humidity sounding channels in clear-sky conditions, the top of the atmosphere radiances, T_B, can be expressed as:

$$T_B = T_s \Gamma \varepsilon + (1-\varepsilon)\Gamma T_{atm}^{\downarrow} + T_{atm}^{\uparrow}, \tag{1}$$

where ε is the surface emissivity, Γ the surface-to-space transmittance, $T_{atm}^{\uparrow}$ the upward atmospheric emission, and $T_{atm}^{\downarrow}$ the downward atmospheric emission inclusive of the microwave background radiation term. This equation is the forward model used for the assimilation of microwave sounder data which are sensitive to the surface. $T_{atm}^{\downarrow}$, $T_{atm}^{\uparrow}$ and Γ are the atmospheric terms which depend on the atmospheric control variables retrieved during the assimilation. In the ECMWF system, the surface skin temperature, T_s, is retrieved separately for each instrument during the analysis in the form of a sink variable. Its background value is taken from the model, with a background error of 5 K over land, 7.5 K over sea-ice and 1 K over ocean. Over ocean the surface emissivity, ε, is calculated at each iteration from the analysed wind and surface temperature fields using the FASTEM model. Over land and sea-ice however, the emissivity must be estimated prior to the assimilation. In order to add ATMS surface-sensitive channels over land and sea-ice we adopted the methods currently used for AMSU-A and MHS, as described in the following.

For AMSU-A, the window channel at 50.3 GHz is used to calculate the emissivity for the temperature sounding channels around 53 - 56 GHz and for MHS, the window channel at 89 GHz is used for calculating the emissivity of the humidity sounding channels in the 183 water vapour band. Following this approach, we selected ATMS window channels at the same frequencies for the land and sea-ice emissivity calculation which are channel 3 for the temperature sounding channels 6 - 9 and channel 16 for the humidity sounding channels 18 - 22. For MHS over sea-ice a correction is applied to the retrieved emissivity and so we applied the same correction to channel 16 of ATMS. This correction accounts for differences in the emissivity at 89 GHz (channel 16) and the emissivity at 183 GHz (channels 18 - 22). It involves subtracting a constant term of 0.01 and adding the difference in brightness temperatures of channels 17 and 16, divided by the skin temperature. Over land an emissivity atlas was maintained for ATMS, as for AMSU-A and MHS instruments, and these are updated every cycle using a Kalman Filter.

The atlas is used to check the retrieved emissivity which could be influenced by instrument noise and errors in model surface skin temperature. If the retrieved emissivity is different by 0.2 or more from the atlas value, it is not used and the atlas value (a kalman filter update from a previous cylce) is used instead. In this case the retrieved emissivity is also flagged as a bad value and the atlas is not updated.

Before assimilating ATMS in the clear-sky system, we must screen out cloud-affected data. Over ocean, this is done using the a first guess check on a window channel combined with liquid water path and scatter index checks - see [2] for more details. The new temperature-sounding data introduced over land and sea-ice were cloud-screened using a first guess check on window channel 5 (52.8GHz): channels 6 - 8 were not used when the first guess departures of channel 5 exceeded 0.7 K. The humidity sounding channels had a different screening over land and sea-ice. Over land channels 16 - 22 were not used if the first guess departures of channel 17 (165.5 GHz) exceeded 5 K and over sea-ice these channels were not used if the first guess departures of channel 16 (88.2 GHz) exceeded 5 K. There was an additional scatter index check over snow-free land where channels 6 - 7 were not used when the 23 - 89 GHz scatter index exceeded 3.0 K. All of these cloud screening checks are the same as those currently used for the equivalent channels of AMSU-A and MHS.

3.3 Assimilation Trial setup

Experiments were run to test the introduction of ATMS surface-sensitive data over land and sea-ice as follows:

- Control experiments: Cycle 39R1 of the ECMWF forecasting system with an additional skin temperature sink variable bug fix (to be made operational in cycle 40R2),
- Land experiments: As control but with the introduction of ATMS humidity channels and ATMS surface-sensitive temperature sounding channels over land,
- Land and sea-ice experiments: As the land experiments but with the additional ATMS channels also added over sea-ice.

Experiments were run for a total of just over 4.5 months over 2 periods: 1 January - 15 February 2013 and 22 April - 31 July 2013. They were run at a resolution of T511, with 137 model levels in the atmosphere.

3.4 Results

As for the HIRS experiments, we assessed the impact of the additional ATMS data by looking at the change in the first guess departures, which indicates the 12-hour forecast fit to observations, and also changes in the forecast scores for temperature, humidity, geopotential and vector wind. For both the land and the land and sea-ice experiments, the standard deviation of first guess departures for MHS and AMSU-A channels 5 - 8 (equivalent of ATMS 6 - 9) was found to be reduced when ATMS data were introduced, indicating an improvement in the 12 - hour temperature and humidity forecasts. This is shown in figures 6 and 7. The reduction was about 0.5% for MHS and 0.05 - 0.1% for the lower-peaking AMSU-A channels and was statistically significant as indicated by the error bars in figures 6 and 7. It can also be seen in these figures that the standard deviation of MHS departures for channel 4 were lower for the ATMS over land and sea-ice experiment than for the ATMS over land experiment, indicating an improved short-term humidity forecast when ATMS data were introduced over sea-ice, as well as over land. For all other instruments the background departures were unchanged.

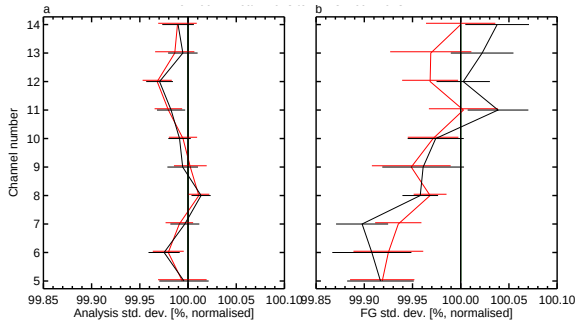

Figure 6: The percentage change in standard deviation of analysis departures (left) and background departures (right) versus channel for AMSU-A used data. Data are averaged globally, over all satellites and for the whole experimental period (1.5 + 3 months) and values are normalised to the control. The red line indicates the 'ATMS over land' experiments and the black line indicates the 'ATMS over land and sea-ice' experiments. Values below 100 indicate a reduction when the new ATMS data is used.

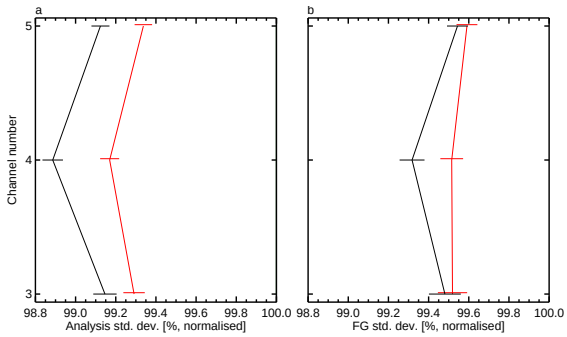

Figure 7: The same as figure 6 but for the MHS instrument instead of AMSU-A.

The change in forecast scores between experiment and control were calculated for geopotential height, temperature, humidity and vector wind for different atmospheric pressure levels and for the 1 - 10 day forecasts, as with the HIRS experiments. These showed a mainly neutral impact for the ATMS over land experiment with respect to the control. As an example, figures 8 and 9, show the ATMS over land geopotential and temperature forecast scores minus control forecast scores, shown in red, and the ATMS over land and sea-ice forecast scores minus control, shown in black. For the ATMS over land and sea-ice experiment we can see here no statistically significant change in forecast scores with the exception of the 1 and 2 day temperature forecasts in the Southern Hemisphere, shown in figure 9 (left). This can be seen more clearly in a global map of the 1 day temperature forecast minus control for the ATMS over land and sea-ice experiment, shown in figure 10, where a large area of negative impact is visible in the Southern Hemisphere ocean. This corresponds to areas of cold sea just North of the sea-ice. ATMS data were added for these areas because in the process of adding data over sea-ice a strict filter was removed which filtered any data with a sea surface temperature of less than 278 K. Instead now we treat any data with a sea surface temperature of less than 271.45 K as sea-ice. The red area in figure 9 corresponds to data being added over sea when the skin temperature is between 271.45 and 278 K. It is not clear why we see this degradation. It may simply be that adding more data has made the analysis more variable rather than degrading the forecast. This is further supported by the fact that forecast scores verified against the operational analysis do not show this signature and the standard deviation of background departures were unchanged for AMSU-A in this area. However we decided to take a cautious approach and not introduce ATMS over sea-ice or cold sea operationally, keeping the same operational set-up over ocean, pending further study.

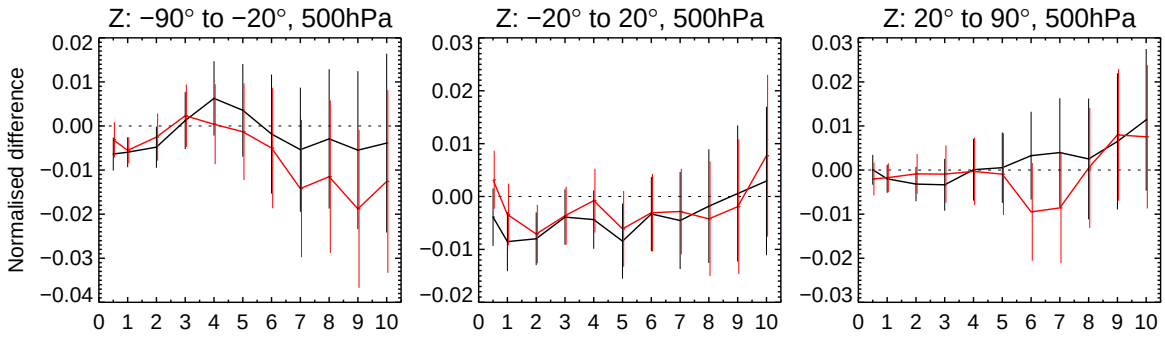

Figure 8: Difference in the root mean square geopotential forecast minus analysis between ATMS experiments and the control as a function of forecast day. Results are verified against own analysis and are averaged over the Southern Hemisphere extratropics (left), tropics (centre) and Northern Hemisphere extratropics (right) at 500hPa. The red line indicates the 'ATMS over land' experiments and the black line indicates the 'ATMS over land and sea-ice' experiments.

3.5 Conclusions

We tested the introduction of ATMS humidity and surface sensitive temperature sounding channels over land and sea-ice into the ECMWF model by performing assimilation trials where the new data were used. To introduce these data we followed methods developed previously for AMSU-A and MHS to estimate the surface emissivity and skin temperature values. Results showed that the introduction of data over land had a positive impact on short-range temperature and humidity forecasts. The introduction of data over sea-ice produced more mixed results. Standard deviation of background departures were reduced for the MHS humidity sounder, indicating an improvement in the 12-hour humidity forecasts, but some negative impacts were observed over the Southern Hemisphere ocean for the 1 day 1000 hPa temperature

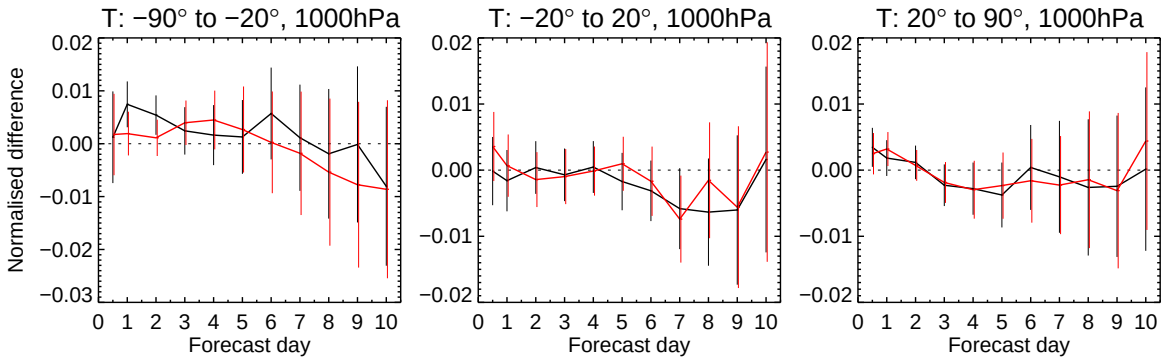

Figure 9: Same as figure 8 but for temperature forecast scores at 1000hPa.

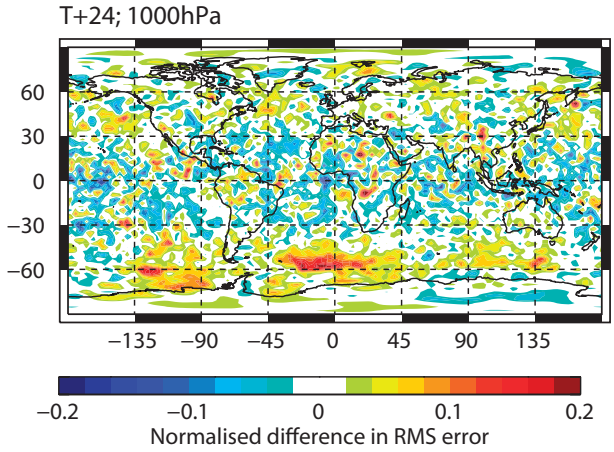

Figure 10: Difference in the root mean square temperature forecast score at 1000hPa for the day 1 forecast: ATMS over land and sea-ice minus control. Red and green colours indicate a reduction in forecast skill between the experiment and control and blue indicates and improvement in forecast skill.

forecast scores. This could be due to a degradation in the temperature forecasts or, since these scores are verified against own analysis, it could indicate a change in the analysis as a result of the addition of new data, which would not necessarily be a concern. As a result of the assimilation trials for ATMS it was decided to make the change over land operational (for cycle 40R3) but not to introduce the data over sea-ice. Work is ongoing to introduce the humidity sounding channels into the all-sky stream at ECMWF and then the introduction of data over sea-ice can be tested again in this stream.

4 Observation Errors for AMSU-A channels 5 - 7

4.1 Introduction

The Advanced Microwave Sounding Unit -A (AMSU-A) measures radiances at different frequencies, which are sensitive to temperature at different heights of the atmosphere. The direct assimilation of these radiances in the ECMWF assimilation system, along with IASI, AIRS and HIRS radiances, and radiosonde data, contributes to the retrieval of atmospheric temperature in the analysis. AMSU-A is an important instrument because we have a very good global coverage of this data type both due to the fact that we are able to use the data in a variety of atmospheric and surface conditions (cloud, sea-ice, etc.) and because we currently assimilate data from 6 individual AMSU-A instruments onboard 6 different satellites, each with a different equatorial crossing time and each sampling a different period of the diurnal cycle.

There are 10 different sounding channels on AMSU-A with frequencies around the 60 GHz oxygen absorption line and the radiances from these channels are sensitive to different parts of the troposphere and stratosphere. Channels 5 - 8 have weighting functions which peak in the troposphere, channel 9 in the tropopause and channels 10 - 14 in the stratosphere. The weighting functions for these channels are the same as channels 6 - 15 for ATMS which are shown in figure 5 (channel 6 ATMS is equivalent to channel 5 AMSU-A, channel 7 ATMS to channel 6 AMSU-A, etc.). The lower peaking AMSU-A channels (5 - 8) are important for weather prediction, particularly channel 5 which peaks at around 700 hPa at nadir (see figure 5), but they are harder to assimilate than the higher peaking channels because they are sensitive to cloud and have a surface emission and reflection component. Because of this we rely on estimates of the surface skin temperature and emissivity and a cloud screening procedure in order to assimilate these radiances in clear sky conditions.

In assimilating satellite data we must establish values of observation errors to assign to each datum, which decides the weight given to the data in the analysis. These values should include instrument noise, forward model error, and error correlation between channels. In practice we assume a constant, uncorrelated value, which is generally inflated above the diagnosed instrument noise value to account for correlations and forward model errors which are otherwise ignored. However [1] recently found that the interchannel error correlations are very low for AMSU-A, which allowed the authors to reduce AMSU-A observation errors used at ECMWF to 0.20 K for channels 6 - 9 and 0.28 K for channel 5, leading to an improvement in forecast accuracy.

Currently AMSU-A observation errors are fixed values for each channel, that is they do not depend on atmospheric or surface fields. However for channels 5 - 8 which are sensitive to surface emission and cloud, there are forward model errors due to uncertainties in these components, which will depend on the atmospheric situation and the surface type. For example we expect emissivity errors to be higher over land than over ocean, and in some cases data will pass the screening in the presence of cloud which will increase forward model error, since cloud effects are not included in the forward model.The aim of

this study is to develop and test new observation errors for AMSU-A channels 5 - 8 which account for forward model errors due to undetected cloud and uncertainties in the surface emission.

Previously [3] developed a simple equation relating errors in skin temperature and emissivity to errors in the calculated top of the atmosphere brightness temperatures, from approximate radiative transfer equations. Looking at AMSU-A channel 5 first guess departures, the author suggested that over land the skin temperature errors dominate and over ocean the surface emissivity errors dominate. For the surface component of the observation errors we will adopt the equation given in [3] but will only consider emissivity error terms since in the ECMWF assimilation system the skin temperature is retrieved in the analysis.

4.2 Observation errors

The total AMSU-A observation error, σ_o, due to instrument noise and forward model error coming from emissivity and cloud terms can be expressed as follows:

$$\sigma_o^2 = \sigma_{emis}^2 + \sigma_{cloud}^2 + \sigma_N^2, \tag{2}$$

where σ_N is the noise term, σ_{emis} the emissivity error term and σ_{cloud} the cloud term. The noise term is a constant value for each channel and the cloud and emissivity terms will depend on characteristics of the surface and atmosphere. The σ_{cloud}-term arises as we currently assimilate AMSU-A using a clear-sky radiative transfer model. Attempts at using the tropospheric AMSU-A channels in all-sky conditions have so far not been successful [4].

4.2.1 Emissivity term

In this study we account for forward model errors due to surface terms by considering the uncertainty in the emissivity. Note that we do not consider skin temperature errors since the skin temperature is a 4D-Var control variable. An error in surface emissivity, $\delta\varepsilon$, will produce an error in the atmospheric radiances of a surface sensitive channel, δT_B which can be expressed as [3]:

$$\delta T_B = (T_s - T)\,\Gamma\delta\varepsilon + (T - T_c)\,\Gamma^2\delta\varepsilon, \tag{3}$$

where we have assumed an isothermal atmosphere of temperature T, and ε is the surface emissivity, T_s is the skin temperature, Γ the surface-to-space transmittance, and T_c is the cosmic microwave background radiation.

From (3) we can see that in the case where surface and atmospheric temperatures T_s and T are similar, the dominant term for the emissivity error is $(T - T_c)\,\Gamma^2$, since $T_c \sim 2.7K$. Thus we can write the emissivity error term σ_{emis} as:

$$\sigma_{emis}^2 = \overline{(\delta T_B)^2} \approx (T - T_c)^2\,\Gamma^4\overline{(\delta\varepsilon)^2}. \tag{4}$$

(4) can also be expressed as a function of the skin temperature:

$$\sigma_{emis}^2 \approx T_s^2\Gamma^4\overline{(\delta\varepsilon)^2}, \tag{5}$$

where we have assumed that $T - T_c \approx T \approx T_s$. Then (2) becomes:

$$\sigma_o^2 = T_s^2 \Gamma^4 \overline{(\delta\varepsilon)^2} + \sigma_{cloud}^2 + \sigma_N^2. \tag{6}$$

This gives us an equation for the observation errors which increases with surface-to-space transmittance, skin temperature and emissivity error, i.e. observation errors are higher where the sensitivity to the surface is higher and for higher surface temperatures. $\overline{(\delta\varepsilon)^2}$ may vary with surface type which means that the observation errors will be different for different surface types. In order to estimate $\overline{(\delta\varepsilon)^2}$ for different surface types we calculated a best fit of (6) where the variance of first guess departures of channel 5 were used as a proxy for σ_o^2, and background values were used for T_s and Γ. We filtered data to remove values which were flagged as cloud contaminated or had liquid water paths $> 0.05 kg/m^2$ over ocean, so that we could assume $\sigma_{cloud} \approx 0$ in (6). We used 1 month of global data, binning $T_s^2\Gamma^4$ values, and calculating the variance of (o-b) for those values over a month. Note that using the first guess departures as a proxy for observation errors in (6) is an approximation since the first guess departures also include skin temperature errors and first guess errors of atmospheric terms as well as other observation error terms including representivity and errors due to undetected cloud. Additionally the ocean emissivity includes first guess errors for the surface wind speed. However performing the fit in this way provides us with an estimate of emissivity errors, which we can check by also comparing them to the variation in retrieved emissivity over different surface types.

Performing a best fit of (6) with $\sigma_{cloud} \approx 0$, we retrieved $\overline{(\delta\varepsilon)^2}$ simultaneously with σ_N^2 for the following surface types: ocean, snow-free land, snow-covered land and sea-ice. Previously [8] calculated values for different types of land surface (desert, forest, etc.) but the values obtained were all very similar, with the exception of snow-cover, and so we decided not to differentiate between these surface types. We checked the validity of the values obtained by calculating the standard deviation of the retrieved emissivities, averaged spatially and over a period of 2 weeks, for different surface types, and these were found to be very similar with the exception of ocean. For ocean the emissivity error calculated from the best fit was 0.20 and the emissivity standard deviation was 0.10. The differences for this value may be due, at least in part, to errors in the first guess wind speed which will increase the first guess emissivity error. However since wind speed is a control variable we do not wish to include this in our emissivity error. We decided to take a value of 0.15 as a compromise.

The final values for $\overline{(\delta\varepsilon)^2}$ are given in Table 4.2.1:

Table 1: emissivity errors for different surface types

Surface Type	$\overline{(\delta\varepsilon)^2}$
Ocean	0.015^2
Sea-ice	0.050^2
Snow-covered land	0.050^2
Snow-free land	0.022^2

4.2.2 Cloud term

Cloud liquid water, rain, ice and snow can affect the radiances of the lower peaking AMSU-A channels by absorption, scattering and/or emission. To illustrate this figure 11 shows the difference in brightness temperatures simulated using the all-sky and clear-sky radiative transfer equations ($T_{B\_all} - T_{B\_clear}$) for

NOAA-19 AMSU-A channels 5 - 7, and for one cycle of the ECMWF forecasting system. Figure 12 shows the corresponding first guess cloud, rain, snow and ice water paths. Here we can see that in the presence of cloud, rain, ice and snow the radiances can be either reduced or increased for channel 5. Generally they are reduced in the tropics and increased in the extratropics, which is likely due to the scattering of ice, snow and/or rain being the dominant mechanism in the tropics and cloud emission dominating in the extra-tropics. The strong positive signatures in the Southern Hemisphere correspond to areas of cloud liquid water with low amounts of rain, ice or snow. Water has less impact on channels 6 and 7 (see the difference in scale for different channels in figure 11) and it is the negative signatures which dominate. Maps of AMSU-A first guess departures in the clearsky stream for one cycle of the ECMWF operational system also show broadly similar patterns, as plotted in figure 13 for NOAA-18 channels 5 - 6 and NOAA-19 channel 7 in the same assimilation cycle as shown in figure 11. For channel 5 we can see some negative scattering signatures in the tropics and some positive signatures in the extra-tropics, very similar to those for the simulated $T_{B\_all} - T_{B\_clear}$, shown in figure 11. However there is also some additional noise in the clear-sky first guess departures, shown in figure 13. For channels 6 and 7 the effect of cloud, rain, ice and snow are less obvious but this may be due to the smaller effects that we expect to see in these channels (see the scale of simulated $(T_{B\_all} - T_{B\_clear})$ in figure 13). It appears that the instrument noise and/or background errors are dominating the first guess departures for channels 6 and 7. Nevertheless some scattering signatures in the tropics can be seen for channel 6.

In the current assimilation of AMSU-A we first screen for cloud-affected radiances and then use the remaining data in the clear-sky stream of the ECMWF assimilation system. The aim of this part of the study is to continue using AMSU-A in the clear-sky stream but to account for forward model errors in the presence of liquid cloud, which mainly change the radiances by the mechanisms of emission and absorption, with an increased observation error. We will do this for data over ocean, since we can calculate a liquid water path over ocean, but not for land or sea-ice. To model the effect of liquid cloud on observation errors, we calculated an empirical fit between the standard deviation of first guess departures and the liquid water path calculated from AMSU-A window channels. The AMSU-A liquid water path is calculated following the method of [5] and is an estimation for the cloud liquid water. The first guess departures before cloud screening were used as a proxy for the observation errors. In this case we assume that errors due to cloud dominate over the emissivity errors in the first guess departures (which is reasonable given the low emissivity error calculated for ocean in section 4.2.1).

Figure 14 shows the standard deviation of first guess departures as a function of binned AMSU-A liquid water path (blue triangles) for channels 5 - 7, averaged over 1 month of data. The different points in these figures indicate values for different satellites and the standard deviation of first guess departures are calculated for liquid water paths binned in intervals of 0.05 kg/m^2. We also calculated the simulated $\overline{(T_{B\_all} - T_{B\_clear})^2}$ from simulated first guess radiances in the allsky stream (T_{B_all}) and clearsky stream (T_{B_clear}) for NOAA-19 AMSU-A. These we combined with a constant noise term (of 0.25 for channel 5 and 0.2 for channels 6 and 7) in order to more easily compare them to first guess departures and they are plotted as a function of liquid water path calculated from simulated AMSU-A allsky radiances as the red dashed lines in figure 14. This figure shows an increase in clear-sky first guess departures with cloud liquid water, which is approximately similar to the increase in simulated $\overline{(T_{B\_all} - T_{B\_clear})^2}$.

Based on these plots we decided to model the cloud observation error term as a quadratic for channels 5 and 6 and as a linear fit for channel 7. We did this for each different satellite and then took values which gave the steepest slope. The resulting regressions were:

channel 5:

$$\sigma_{cloud} = 2.0 lwp^2 + 0.79 lwp, \tag{7}$$

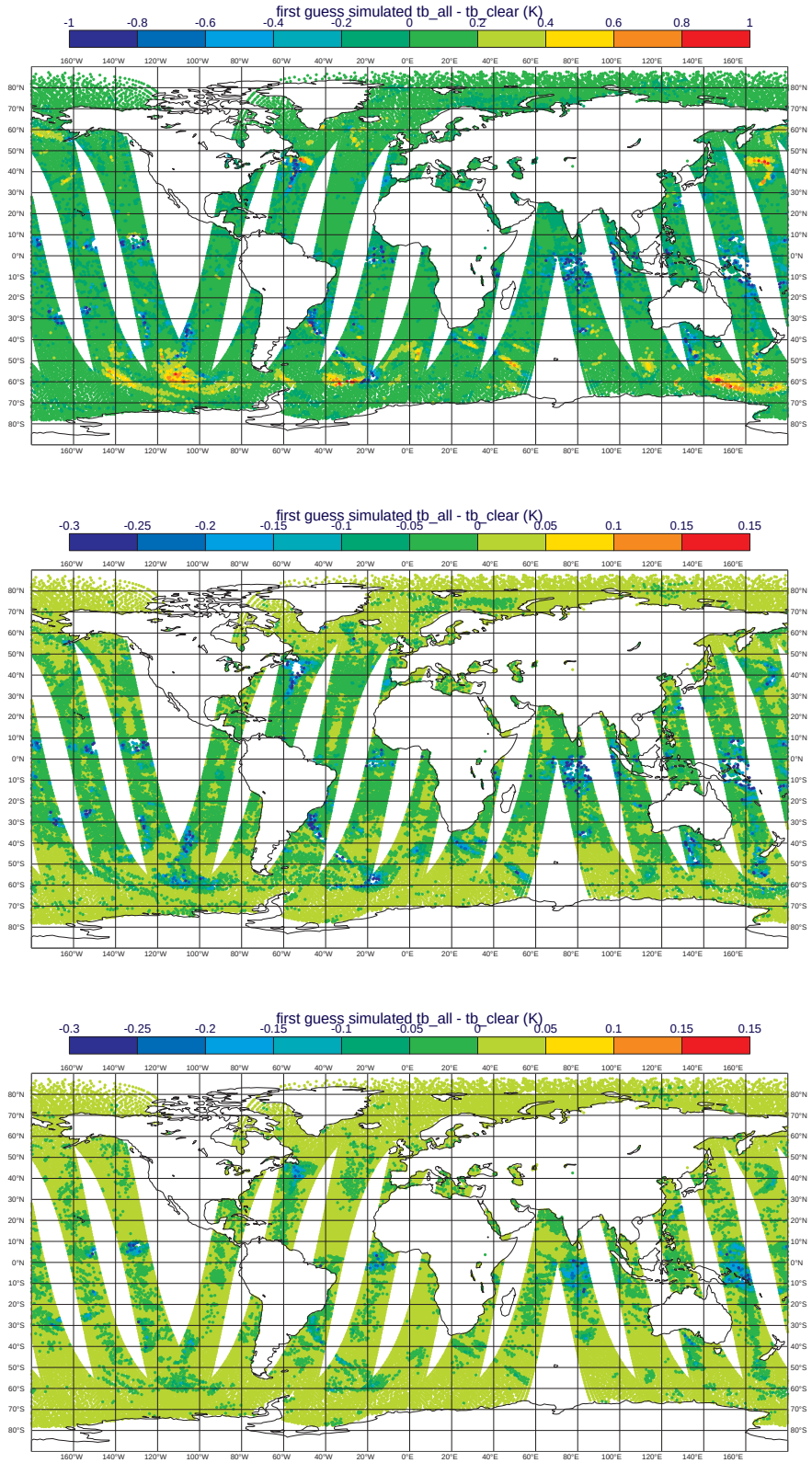

Figure 11: Difference in simulated radiances calculated using the all-sky radiative transfer equations (T_{B_all} calculated with RTTOV_SCATT) and clear-sky radiative transfer equations (T_{B_clear} calculated with RTTOV) for AMSU-A channels 5, 6, 7 (top-to-bottom)

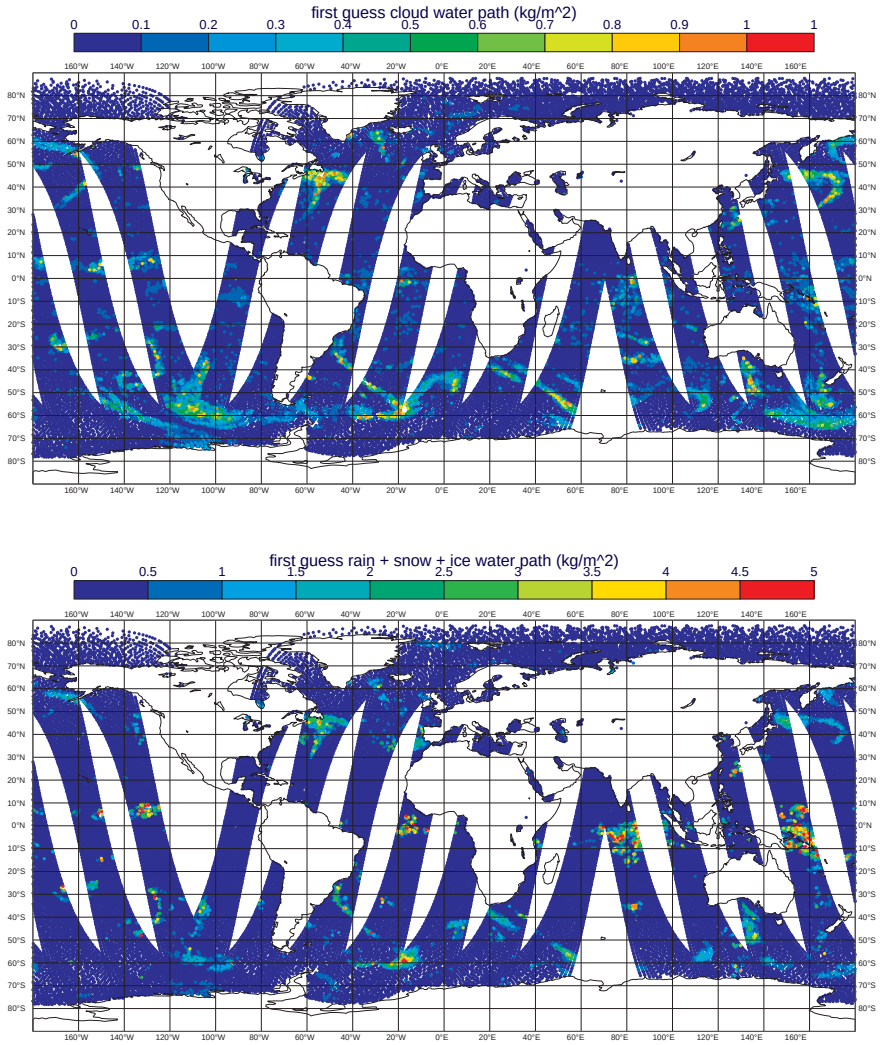

Figure 12: first guess cloud water path (top), and rain + snow + ice water path (bottom)

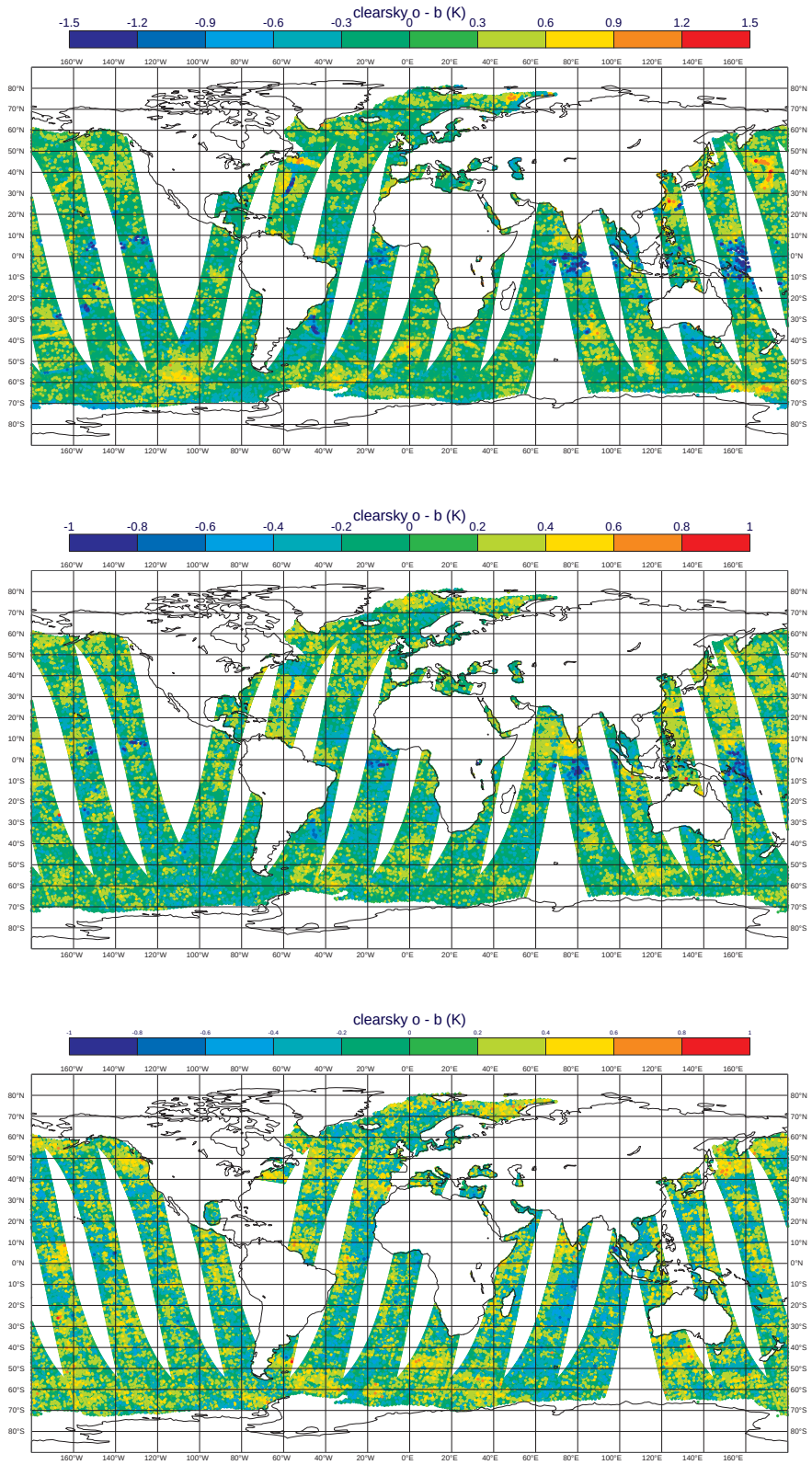

Figure 13: First guess departures for channels 5, 6 for NOAA-19 and channel 7 for NOAA-18 (top-to-bottom) in the ECMWF clearsky stream.

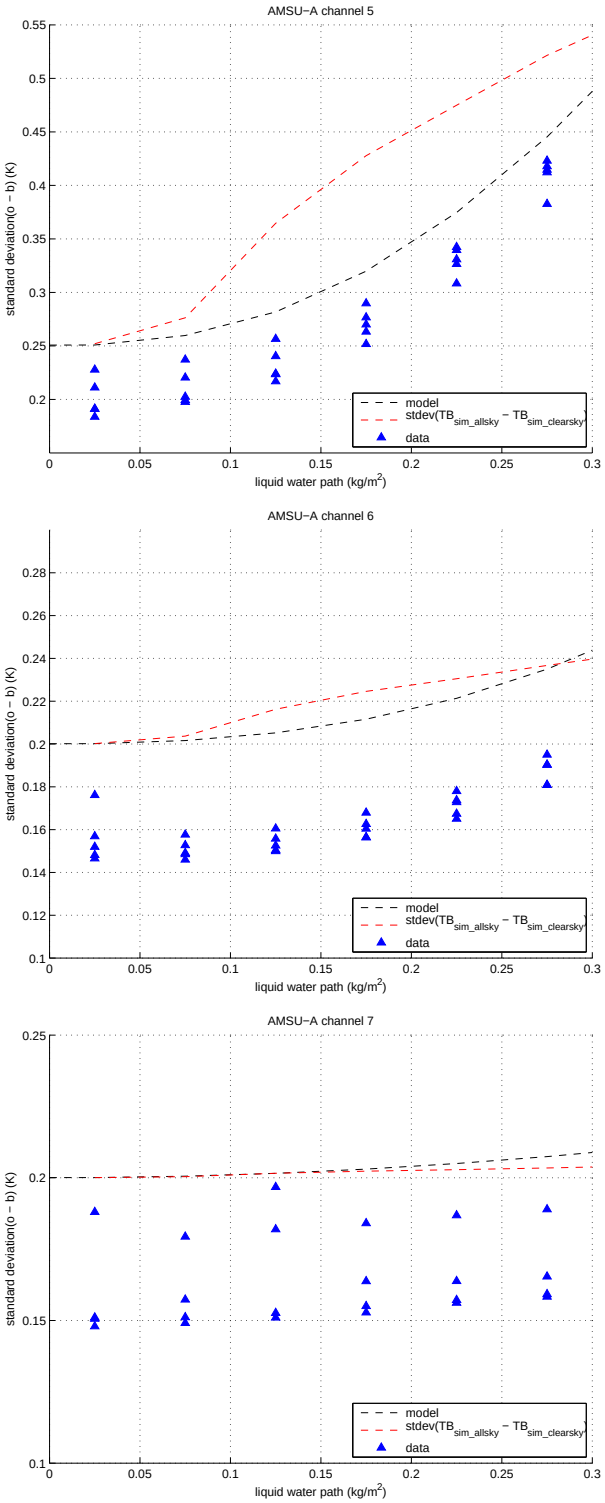

Figure 14: Standard deviation of clear-sky background departures as a function of liquid water path (blue triangles) for channels 5 - 7 (top-to-bottom) of AMSU-A. Also shown are the best fits (black dashed line) and the simulated $T_{B\_all} - T_{B\_clear}$ as a function of first-guess simulated liquid water path (red dashed line).

channel 6:

$$\sigma_{cloud} = 0.54lwp^2 + 0.30lwp, \tag{8}$$

channel 7:

$$\sigma_{cloud} = 0.20lwp. \tag{9}$$

These best fits are shown in figure 14 as the dashed black line, with an additional noise term of 0.25 K for channel 5 and 0.20 K for channels 6 and 7.

The background departures used for these fits include all data and so will be affected by scattering of ice, snow, and rain as well as the absorption/emission effects of liquid water. The ice, snow and rain water paths are likely to be correlated to the liquid water path and so may be affecting the best fits (7) - (9) for the different channels. The could explain the dependence of background departures on liquid water path for channels 6 and 7 since for these channels the radiances are mainly affected by the scattering of rain, ice and snow rather than the emission/absorption signatures of cloud liquid water.

The approach used here to develop a liquid water path-dependence on observation errors is an empirical one. However it might be possible to apply a more physical method, such as the one applied for the emissivity errors. The advantage of applying an empirical method is that we avoid problems due to approximations and assumptions in the physical approach but the disadvantage could be that we are over-fitting to data which is affected by scattering, emissivity errors, first guess errors, etc. as well as the liquid water path. In the future it could be interesting to try a more physical approach, and test both with assimilation trials.

4.3 Noise term

Constant noise terms were calculated for each satellite as the intercepts while performing the regressions for the cloud term and for the surface term described in sections 4.2.1 and 4.2.2. These values were different for each satellite/channel combination, as we would expect, but we decided to use a constant term for each channel, which we chose to be the highest noise term. In the future we could reduce the AMSU-A observation errors for some satellites. We chose the following values:

channel 5:

$\sigma_N = 0.25K$,

channels 6 and 7:

$\sigma_N = 0.20K$.

This keeps the same noise term for channels 6 and 7, as are currently used, and reduces the noise value for channel 5 from 0.28 K to 0.25 K. However we now also have additional surface and cloud terms for all three channels.

4.4 Cloud quality control over ocean

Currently AMSU-A channel 5 - 8 data are filtered for cloud contamination before being assimilated in the clear-sky stream. The liquid water path is used for screening channels 5 and 6 over ocean - data are not used if values exceed 0.30 kg/m^2. There is also a window channel check where if the first guess departures of the 50.3 GHz channel (channel 3) over ocean are higher than 3 K (absolute values) we

assume cloud contamination and remove channels 5 - 7 and channel 8 in the tropics (latitude $< 30°$). Now that the observation errors increase with liquid water path we may be able to remove this window channel check and thus introduce more data, which would be downweighted by the liquid water path term. However we still want to filter for strong scattering effects since this is not accounted for in the observation error and in any case strong scattering would introduce local biases. In order to do this we envisage using the scatter index, which is calculated as the radiances of channel 1 (23 GHz) minus channel 15 (89 GHz). To choose the scatter index threshold we plotted the first guess departures of channel 5 as a function of the scatter index. Essentially we want to remove all strongly negative first guess departures which are indicative of scattering. This is shown in figure 15 for channels 5 and 6 (data from all satellites combined).

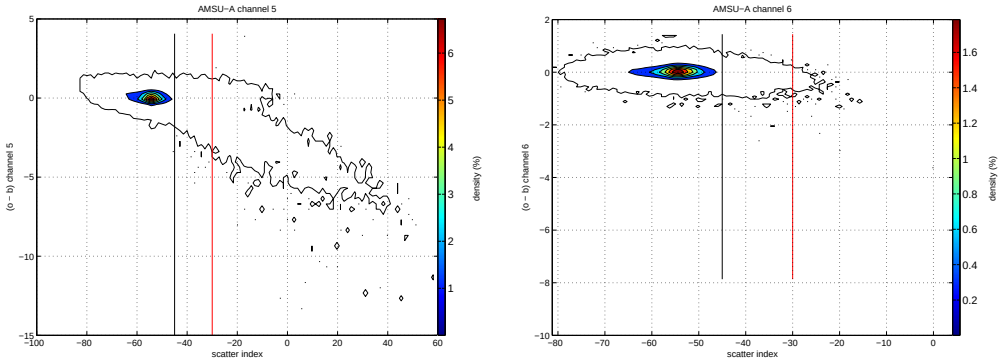

Figure 15: Clear-sky first guess departures as a function of scatter index for left) channel 5 and right) channel 6

From figure 15 we selected two possible thresholds where data are kept either for a scatter index $<$ -45 K or a scatter index $<$ -30 K. These two thresholds are plotted in the figure as black and red lines respectively. Note that these thresholds will also remove data in areas of high snow, ice and rain water paths. We decided to test both threshold possibilities in assimilation trials.

We also want to be sure that this scatter index threshold prevents us from introducing strong local biases when we relax the first guess cloud check. Figure 16 shows the mean first guess departures for channels 5 and 6 for different latitudes, before and after the scatter index $<$ -30 K and scatter index $<$ -45 K checks. We can see from this that before filtering we have a strongly negative bias for channel 5 in the tropics due to scattering and a smaller positive bias in the extratropics due to cloud water emission. The scatter index check at -30 K reduces the negative bias in the tropics, and it is even more reduced for the scatter index check at -45 K. The positive bias for channel 5 in the extratropics is not affected however. The residual biases for channel 5 after the scatter index check could still have a negative effect on forecast accuracy, but this can be tested with the assimilation trials.

4.5 Assimilation Trials

In order to test the new observation errors we performed a number of different assimilation trials, each for a period of two months or more. Firstly we tested the new observation errors in the ECMWF data assimilation system without any change to the screening for AMSU-A channels 5 - 8. Secondly, we investigated adding more data in difficult areas where observation errors are higher, with the hope that the new observation errors would downweight these data in such a way that it still provides valuable atmospheric temperature information but that the problems in the forward model are not aliased into the analysis. We have attempted to add more data in cloudy regions, over high topography and over the Southern Hemisphere sea-ice (channel 5). The assimilation trials were as follows:

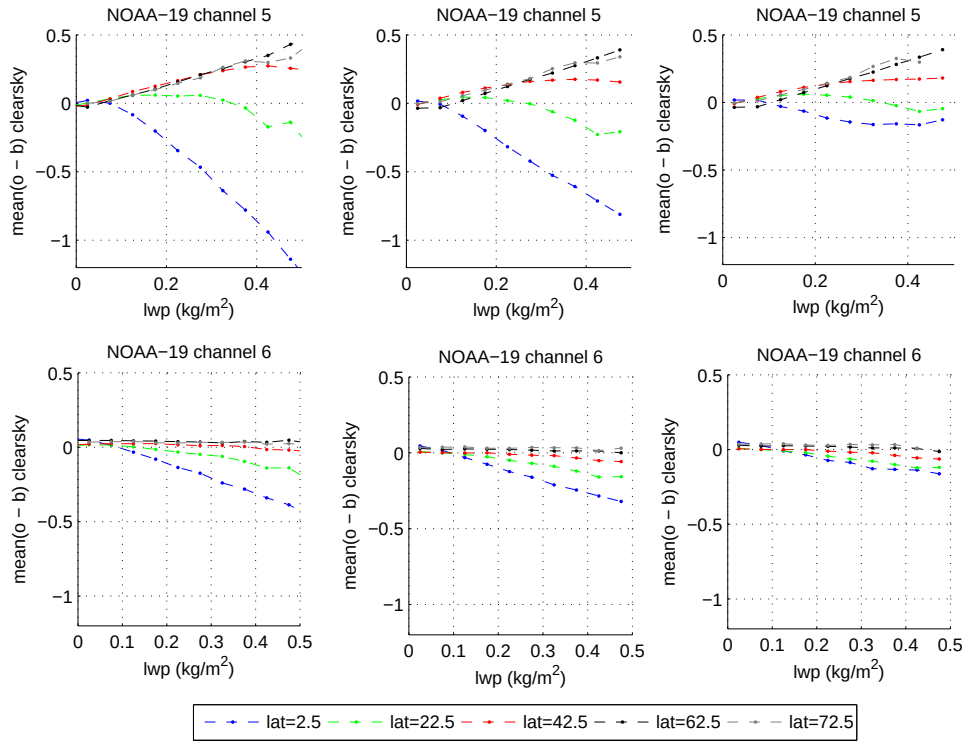

Figure 16: mean (o - b) of NOAA-19 AMSU-A channel 5 (top) and channel 6 (bottom) averaged over a month for different latitudes for: left) all data, middle) all data filtered for scatter index < -45 K, right) all data filtered for scatter index < -30 K

- Control: ECMWF data assimilation and forecasting model with no change to the AMSU-A observation errors

- New observation errors: Same as control but with new observation errors for AMSU-A channels 5 - 7

- New observation errors + sea-ice: Same as 'New observation errors' but with channel 5 data introduced over sea-ice in the Southern Hemisphere (it is currently blacklisted here)

- New observation errors + high orography: Same as 'New observation errors' but with orography screening removed over high topography. Instead an observation error screening was applied which removed all data for channel 5 with observation errors above 0.35 K and channel 6 with observation errors above 0.28 K. Note that since the surface-to-space transmittance is higher over high orography the observation errors will also be higher in these areas.

- New observation errors + cloud 30: Same as 'New observation errors' but with the cloud screening changed over ocean. The window channel check was removed and replaced with a scatter index check for channels 5 - 7 and channel 8 in the tropics (latitude$<30°$), where data were not used if the scatter index was above -30 K. The liquid water path check was kept so that only data with the liquid water path less than 0.3 kg/m^2 was used for channels 5 and 6.

- New observation errors + cloud 45: Same as 'New observation errors + cloud 30' but with a tighter scatter index check at -45 K.

Trials were all run at a horizontal resolution of T511 ($\sim$ 40 km) and with 137 model levels in the vertical and they were run in some cases for the 40R2 version of the ECMWF model and in some cases for 40R1 with some contributions to 40R2. These two versions have only technical differences and in any case two controls were run for each model and each experiment was compared with its corresponding control. In all cases both winter and summer experiments were run in the periods June - September 2013 and December - February 2014 (each 2 - 3 months), except for 'New observation errors + sea-ice' where only a 3 month Southern Hemisphere winter experiment was performed because there is more Southern Hemisphere sea-ice in this season.

4.6 Results

4.6.1 New observation errors with no change in screening

The new observation errors are shown for MetOp-B AMSU-A channels 5 - 7, for the first cycle of the summer 'New observation errors' experiment, used data only. The highest values are for areas of high liquid water path in the Southern Hemisphere. These are areas where the data pass the first guess check on channel 3: other areas of high liquid water path in the tropics do not pass this screening. For channel 5 we can see that the observation error is higher in the centre of the swath, where angles are closer to nadir, so that more weight is now given to the edge of the scanlines and less weight to the scanline centres. This is because the surface-to-space transmittance in (5) is higher for observation angles closer to nadir. This variation of observation error across the swath is small for channels 6 and 7 since they have less overall sensitivity to the surface. For these channels the liquid water path errors dominate the surface errors.

The new observation errors on average gave more weight in the analysis to channel 5 and slightly less weight to channels 6 and 7, since the standard deviation of analysis departures were reduced for channel 5 and increased for channels 6 and 7 when compared to the control. The increase for channels 6 and 7 was to be expected since we chose not to reduce the noise value but only added new terms to the observation errors. However in the future we plan to revisit the noise term, reducing it for different instruments.

The new observation errors overall did not change forecast scores significantly: as an example the change in forecast scores for geopotential at 500hPa and temperature at 1000hPa are given in figure 18. Departure statistics of other satellite instruments and radiosondes were also mainly unchanged, with the exception of a slight increase in standard deviation of first guess departures of ATMS channel 8 in the summer experiment (equivalent to AMSU-A channel 7). This can be seen in figure 19 which shows the change in standard deviation of ATMS background departures for the summer and winter experiments. Note that values for ATMS channels 6 - 8 and 18 - 22 are only averaged over ocean since in this version of the ECMWF forecasting system ATMS is only assimilated over ocean for these channels. The increase in the standard deviation of (o - b) for channel 8 could be due to the observation errors for AMSU-A channels 6 and 7 now being slightly too large for some instruments so that the analysis does not pull as closely to the observations for AMSU-A (and thus AMSU-A-like ATMS). However the increase is very small.

4.6.2 Introducing channel 5 data over Southern Hemisphere sea-ice

Introducing channel 5 over the Southern Hemisphere sea-ice produced a 6 % increase in used data for this channel over the period 15 June - 14 September 2013. The mean observation error for channel 5 over sea-ice was 0.29 K, varying from 0.26 K at the edge of the scanline to 0.34 K close to nadir.

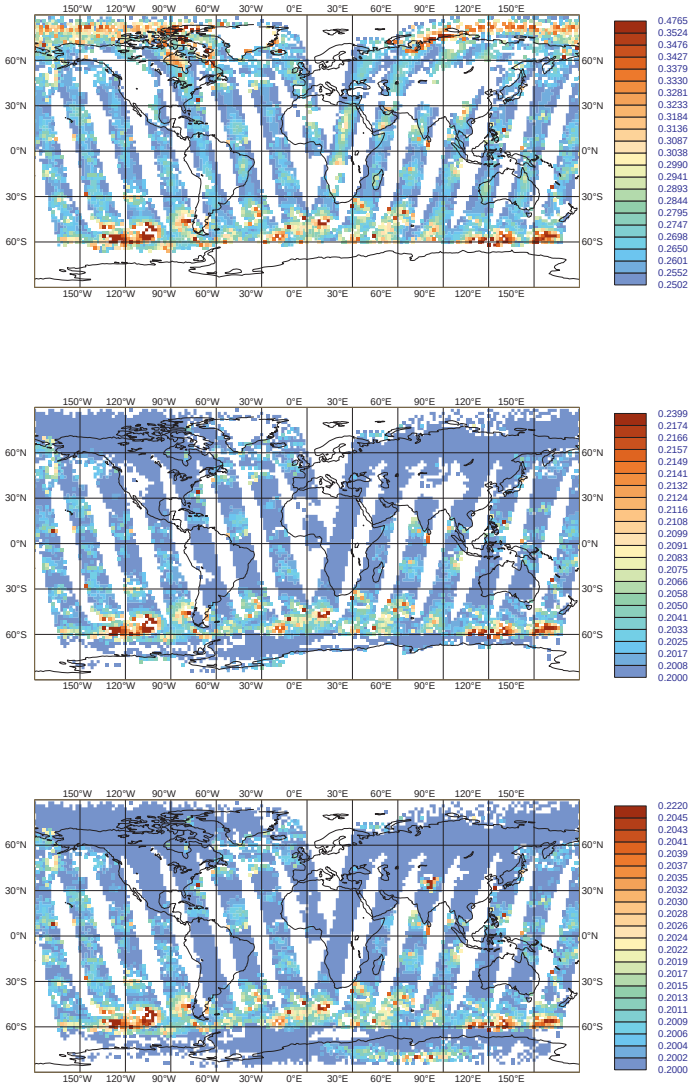

Figure 17: Map of the MetOp-B AMSU-A observation errors for the first cycle of the 'New observation errors' summer experiment for channels 5 - 7 (top to bottom).

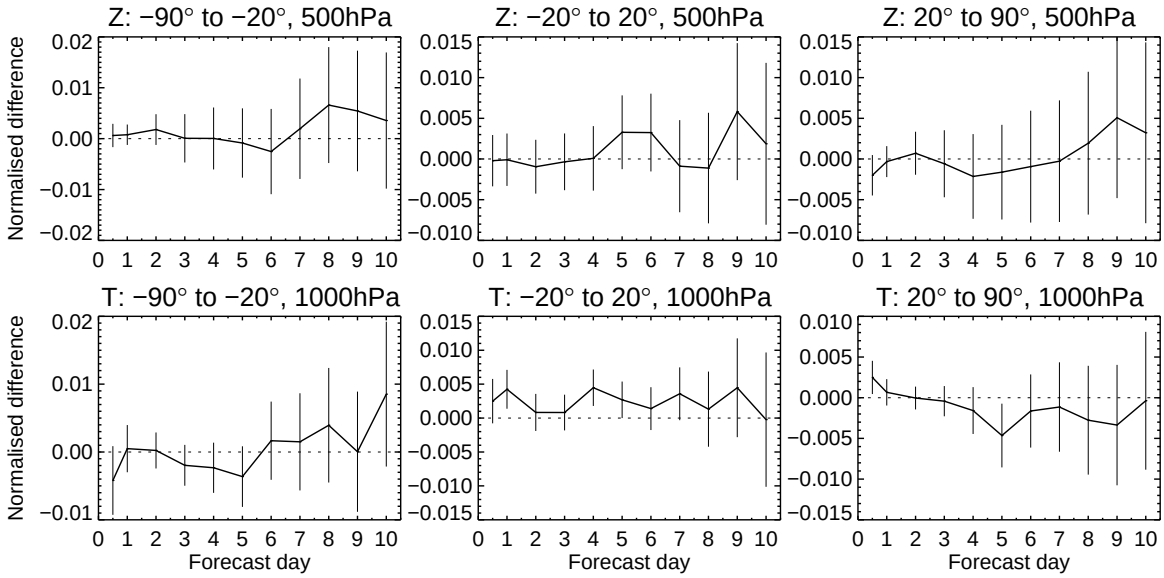

Figure 18: Difference in the root mean square geopotential forecast minus analysis (top) and the root mean square temperature forecast minus analysis (bottom) between 'New Observation Error' experiment and the control as a function of forecast day. Results are verified against own analysis and are averaged over the Southern Hemisphere extratropics (left), tropics (centre) and Northern Hemisphere extratropics (right) at 500hPa over 6 months and both seasons.

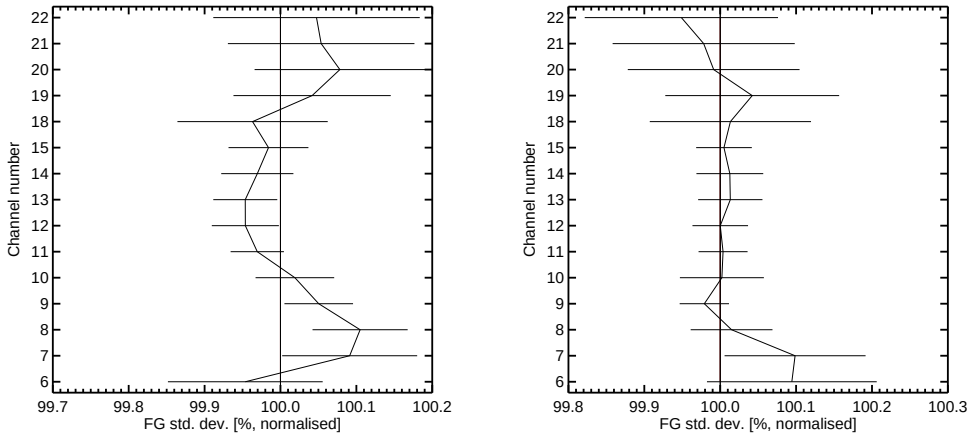

Figure 19: Change in the standard deviation of background departures for ATMS for left) the June - August 2 month period and right) December - January 2 month period: 'New Observation errors' - 'Control'

The change in root mean square temperature and geopotential forecasts minus analysis averaged over the Southern Hemisphere are shown in figure 20 but the scores for the other variables look similar. Shorter range forecast scores (days 1 - 4) were either unchanged or the differences were not statistically significant. However there were some negative impacts around 500hPa at longer ranges (days 6 - 10). Maps of the 500 hPa temperature forecast scores (not shown) indicated that the long-range degradation of temperature scores came from the Southern Hemisphere ocean.

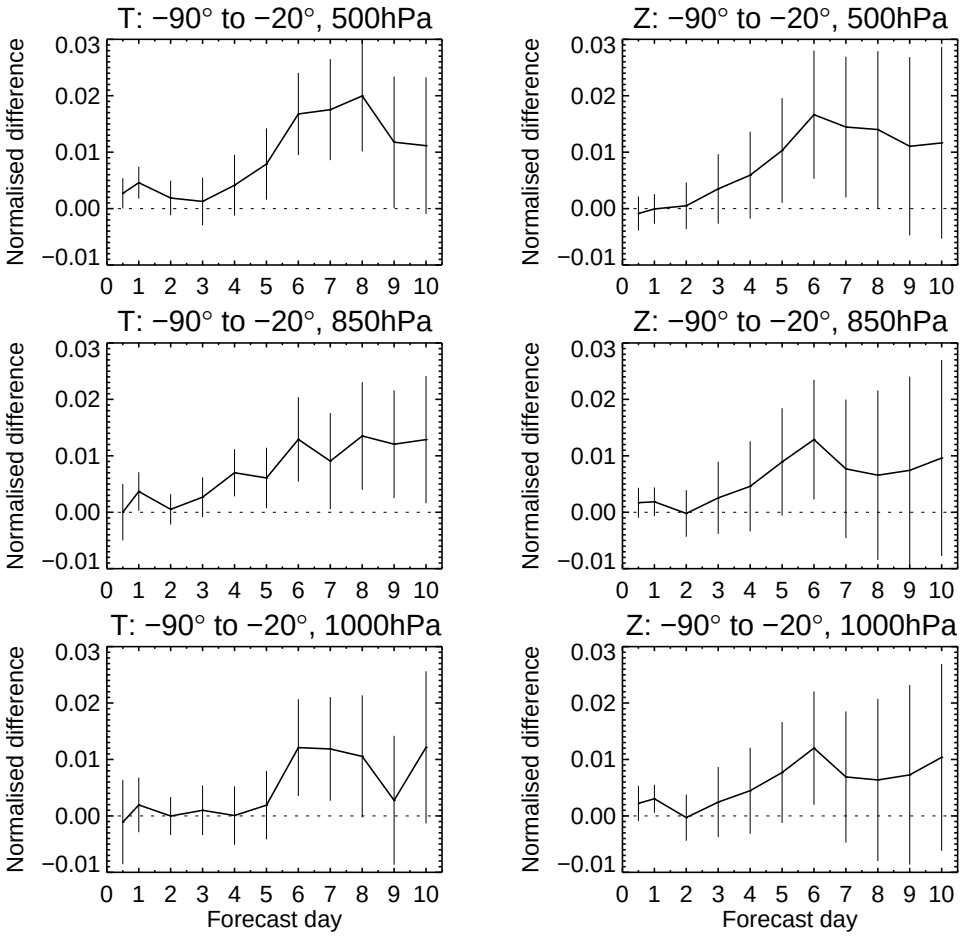

Figure 20: Change in root mean square temperature (left) and geopotential (right) forecast minus analysis over the Southern Hemisphere between New Observation Error experiment + sea-ice (summer 40r1) and the control. Values are shown as a function of forecast day and at 1000 - 500 hPa heights.

The fits of observations to the 12-hour forecast were improved for some instrument/channel combinations and degraded for others, as shown in figure 21. HIRS channels 6 and 14 were improved by 0.1 and 0.5 % respectively over the Southern Hemisphere, and these are low-peaking Infra-Red sounding channels sensitive to atmospheric temperature which are used globally, including over sea-ice. However there was also a statistically significant degradation in the humidity TEMP radiosonde standard deviation of background departures of 2% over the Southern Hemisphere and the microwave humidity sounder MHS showed a slight, statistically significant, degradation for its lowest peaking channel, channel 5, over the Southern Hemisphere of around 0.1 %. Since this MHS channel is not used over sea-ice this degradation comes from the Southern Hemisphere ocean.

The new data added over sea-ice had a high bias in some cases: for NOAA-19, MetOp-A and MetOp-B

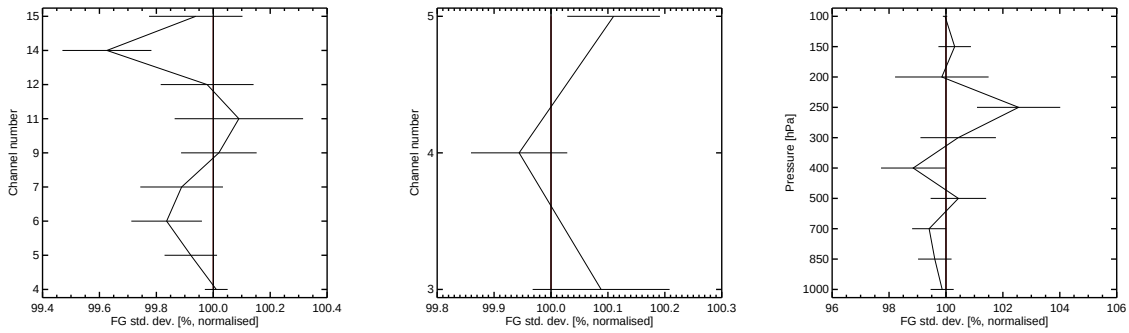

Figure 21: Percentage change in departure statistics over the Southern Hemisphere extra-tropics(x-axis) of the (left-to right) HIRS instrument, MHS instrument and the TEMP humidity radiosondes as a function of channel number (y axis) for the 'New observation errors + sea-ice' minus control experiments. Values are averaged over 3 months of experimentation. Negative values indicate a reduction in standard deviation of background departures when new observation errors are used and channel 5 data is introduced over the Southern Hemisphere sea-ice.

the mean background departures after bias correction were approximately 0.1 - 0.15 K, which is 5 times higher than the typical bias over land and 10 times higher than over ocean. To illustrate this, figure 22 shows the mean background departures for MetOp-B channel 5 (a monthly average after bias correction). As a result of the new data the mean temperature analysis at 1000 - 850 hPa was changed over sea-ice by up to 0.1 K and the mean humidity by up to 0.3 % at 850 hPa. This is shown in figure 23. The introduction of biased data over sea-ice in the Southern Hemisphere will have a higher impact on the analysis than in another part of the Globe, since the background errors are higher making the analysis less constrained by the background, and we also have less radiosonde data to constrain the analysis and anchor the radiance bias corrections here. It is therefore likely that the degradation in the long-range forecast scores, and the degradation in departure statistics for MHS and radiosondes, are due to the introduction of data in the South Pole which are biased relative to the model.

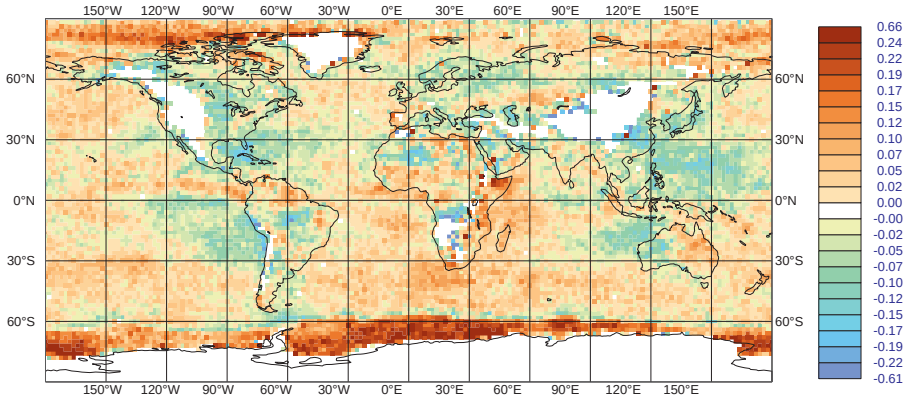

Figure 22: Map of the mean background departure for MetOp-B AMSU-A channel 5 for the 'New Observation Error experiment + sea-ice' experiment. Values are after bias correction and averaged over 1 month from 15/08/2013 - 14/9/2013 (the second month of experimentation).

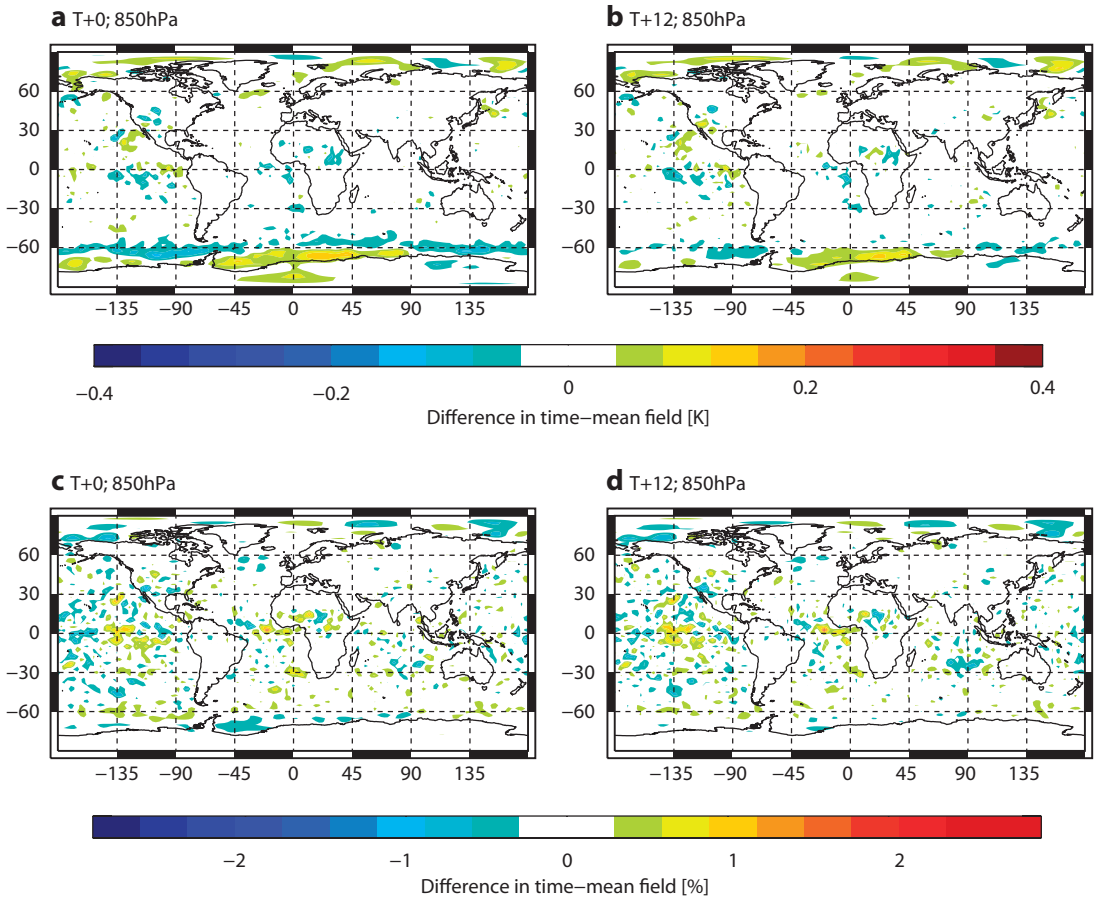

Figure 23: Map of the change in mean 850hPa temperature (top) and humidity (bottom) analysis at 0 hour (left) and 12 hours from the start of the assimilation window between the 'New Observation Error experiment + sea-ice' experiment and the control.(Note the difference in scale).

4.6.3 Introducing channel 5 and 6 data over high orography

Figure 24 shows areas where data were added in the 'New observation errors + high orography' experiment for MetOp-B channels 5 and 6 (MetOp-B is given as an example but there are similar plots for all AMSU-A instruments). The total number of used data increased by 4% for AMSU-A channel 5 and 1.5% for AMSU-A channel 6. Note that some channel 5 data were removed over the Southern Hemisphere ocean in the June - September period due to the observation error check which was introduced globally and removed data in areas of high liquid water path during this period. The number of used data for AMSU-A channel 5 was reduced by 1.5 % over the Southern Hemisphere extra-tropics in this period.

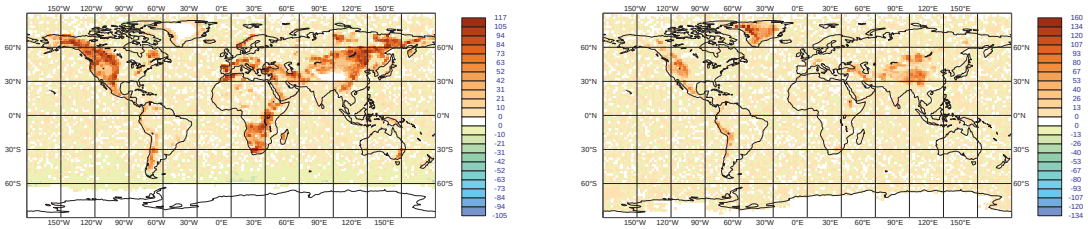

Figure 24: Map of the change in number of used data for MetOp-B AMSU-A channel 5 observation errors between the 'New observation errors + high orography' and control experiments. Red areas show an increase in used data and green areas a reduction.

The introduction of the new data reduced the mean analysis temperature at 500hPa over Greenland by up to 0.05 K, as shown in figure 25. The mean analysis was not affected over other areas of high orography.

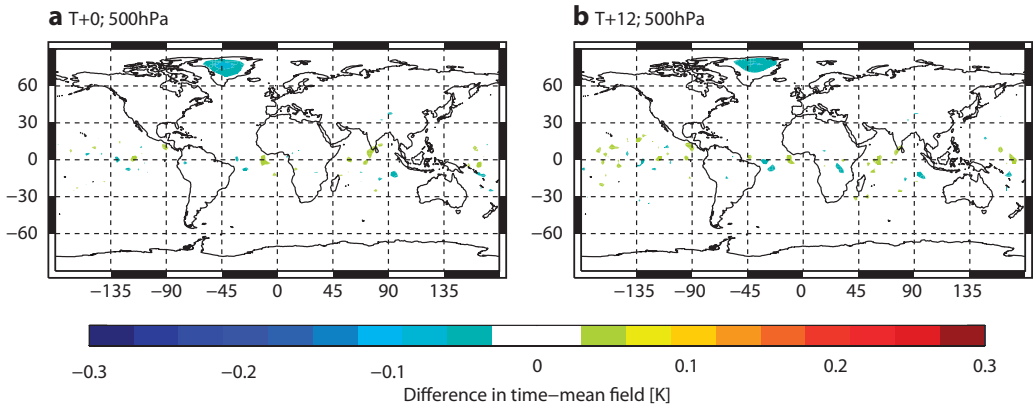

Figure 25: Map of the change in mean 500hPa temperature analysis at 0h (left) and 12h (right) between the 'New Observation Error + high orography' experiment and the control.

The effect of introducing new data over high orography on forecast scores is shown in figure 26 for temperature at 1000hPa and geopotential height at 500hPa for the December 2013 - February 2014 period. The change in forecast scores was neutral when averaged globally for the June - August 2013 period. As figure 26 shows, for the December 2013 - February 2014 period the scores were mainly neutral but there was some degradation in the temperature and wind forecast scores over the tropics at 500hPa. Maps of these forecast scores show that the areas of a negative impact are over the ocean, as shown in figure 27 (right). For comparison the same plot is shown for the 'New Observation Error' experiment (left). Note that the scale is different for each plot. The negative impact over the tropical

ocean at longer ranges could be propagated from forecast errors over high orography at shorter ranges (e.g. days 1 - 3) but it is difficult to make this link when looking at maps of forecast scores, particularly in scores verified against own analysis which can be affected by variable analyses in the shorter ranges when there is additional data. Departure statistics for other satellite instruments were mainly neutral. Temperature radiosonde globally averaged departures were mixed: in June - August period they were somewhat improved around 1000hPa (near the surface) for the AIREP observations but were degraded at around 400hPa for the TEMP radiosondes. In the December - February period some of the departure statistics for wind radiosondes were improved and all others were neutral.

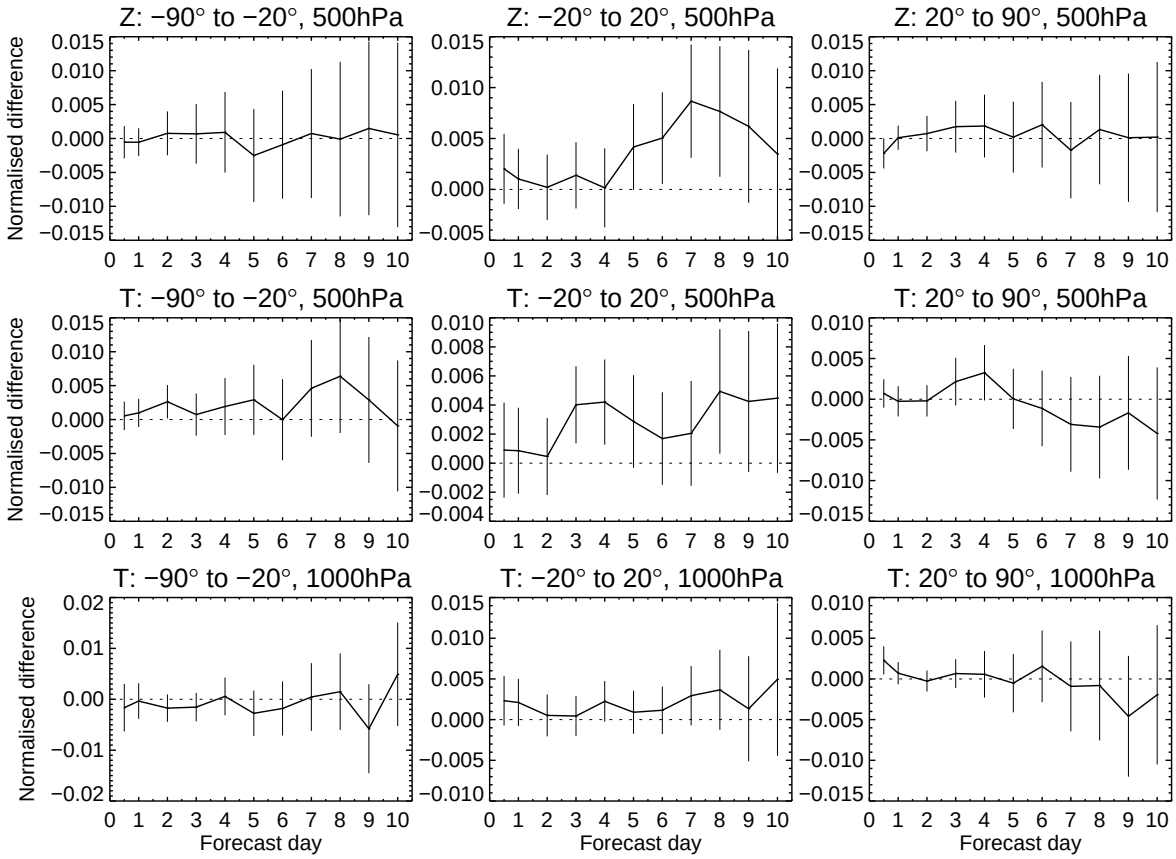

Figure 26: Difference in the root mean square 500hPa geopotential forecast minus analysis (top) and the root mean square 500hPa and 1000hPa temperature forecast minus analysis (middle and bottom respectively) between 'New Observation Error + high orography' experiment and the control, as a function of forecast day. Results are verified against own analysis and are averaged over the Southern Hemisphere extratropics (left), tropics (centre) and Northern Hemisphere extratropics (right) at 500hPa over 5 months in the combining the 15 June - 14 August 2013 and December 2013 - February 2014 periods.

To focus on the impact over high orography we calculated the change in radiosonde standard deviation of (o - b) over areas of high orography where new data were introduced. These are shown in figures 28 - 29. On the whole the changes in standard deviation of background departures for radiosondes over high orography were not statistically significant, as indicated by the errors bars in figures 28 - 29.

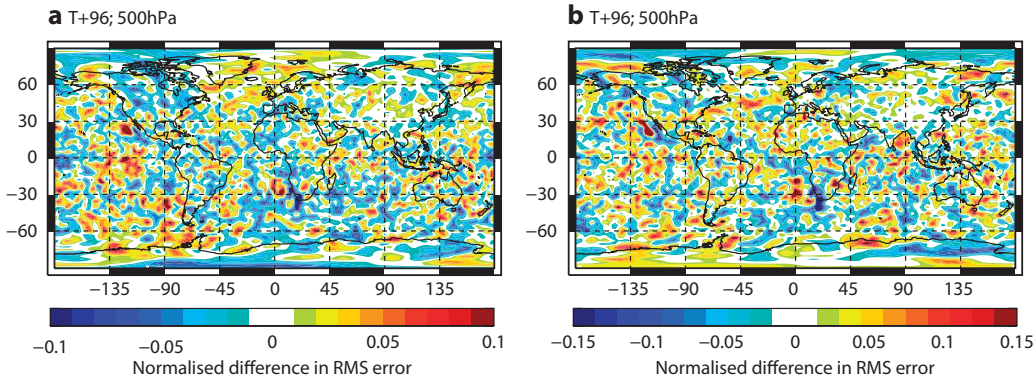

Figure 27: Left) Difference in the root mean square 500hPa temperature forecast minus analysis between 'New Observation Error' experiment (summer 40r1) and the control for day 4 forecasts. Right) Same as left but for the 'New Observation Error + sea-ice' experiment

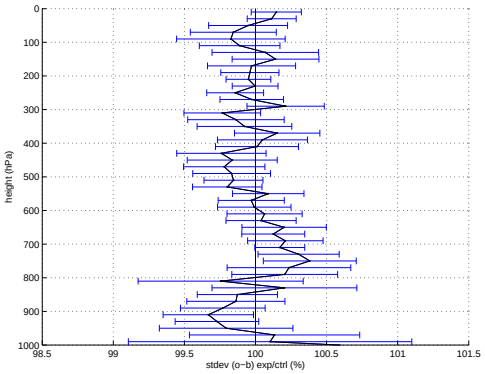

Figure 28: Change in the standard deviation of background departures for radiosondes over high orography for Temperature, shown as exp/control in %. Values averaged over 3 months for December 2013 - February 2014.

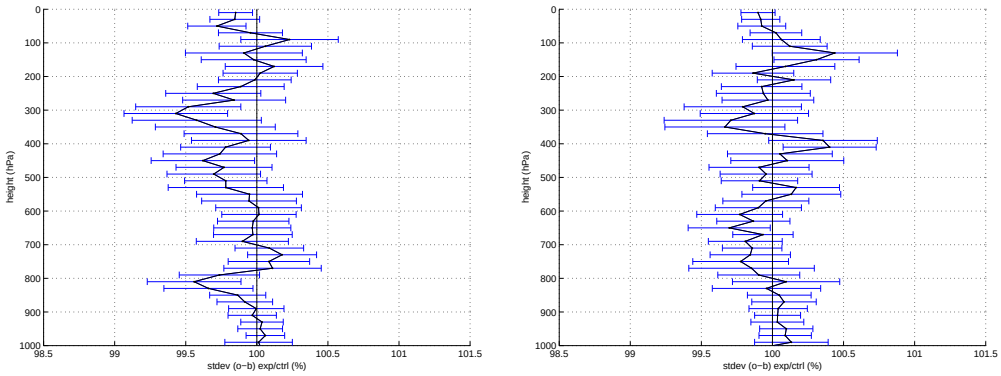

Figure 29: Change in the standard deviation of background departures for radiosondes over high orography for left-to-right u wind component and v wind component, shown as exp/control in %. Values averaged over 3 months for December 2013 - February 2014.

4.6.4 Introducing data in cloudy conditions

Two experiments were run with a modified cloud screening over ocean for AMSU-A channels 5 - 8, on top of the new observation errors. The first guess check on channel 3 over ocean was removed and replaced by, in the first instance, a scatter index check of -30 K ('New observation errors + cloud 30' experiment), and in the second instance a scatter index check of -45 K ('New observation errors + cloud 45' experiment), which removes more data in the tropics. Currently results of the -45 K scatter index check experiment are only available for the period of December 2013 - February 2014.

As a result of the change in screening the total number of used AMSU-A data increased by 13 % for channels 5 - 7 and 3 % for channel 8 for the 'New observation errors + cloud 30' experiment, with respect to the control. For the 'New observation errors + cloud 45' experiment the total number of used AMSU-A data increased by 8 - 9 % for channels 5 - 7 and approximately 0.5 % for channel 8. However in the tropics the number of used data was reduced by 2 - 3 % for channels 5 - 8 for this experiment. This is shown in figure 30.

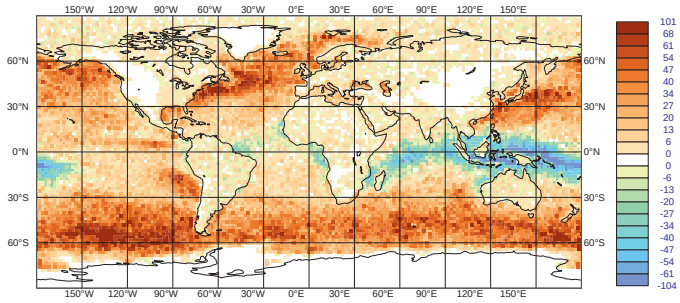

Figure 30: Map of the change in the number of used data for MetOp-B AMSU-A channel 5 between the 'New observation errors + cloud 45' and control.

The first guess departures were mainly unchanged with the introduction of new data, with the exception of ATMS. For the summer 'New observation errors + cloud 30' experiment there was a reduction in the standard deviation of observation fit to 12-hour forecast for ATMS channels 6 - 8, as shown in figure 31. This is encouraging since ATMS has channels of the same frequency as AMSU-A but there was no change to either the observation errors or cloud screening for ATMS. So it appears that the new data introduced agrees well with the non-cloudy ATMS data and is reinforcing it. There was also a reduction in ATMS standard deviation of (o - b) for the 'New observation errors + cloud 45' but this was not statistically significant (see figure 31 right).

Results of the change in forecast scores are shown in figure 32 for both the 'New observation errors + cloud 45' minus control and 'New observation errors + cloud 30' minus control. The 'New observation errors + cloud 30' experiment had a neutral impact on forecast scores in most cases. There was a negative impact on geopotential in the tropics but it is hard to rely on this because since geopotential height is very homogeneous in the tropics, changes in the geopotential forecast scores here are often due to a change in the mean analysis value in the tropics rather than an improvement or degradation in forecast skill.

The 'New observation errors + cloud 45' experiment produced an improvement in the area averages of root mean square forecast scores, particularly for the Southern Hemisphere geopotential as shown in figures 32 (top) and 33 (top). The only negative impact was observed on the short-range temperature forecasts in the Southern Hemisphere ocean, which is shown in figure 32 (bottom). This signature persists to the day 2 forecasts and there are traces of it in the day 3 forecasts and can be observed to come from

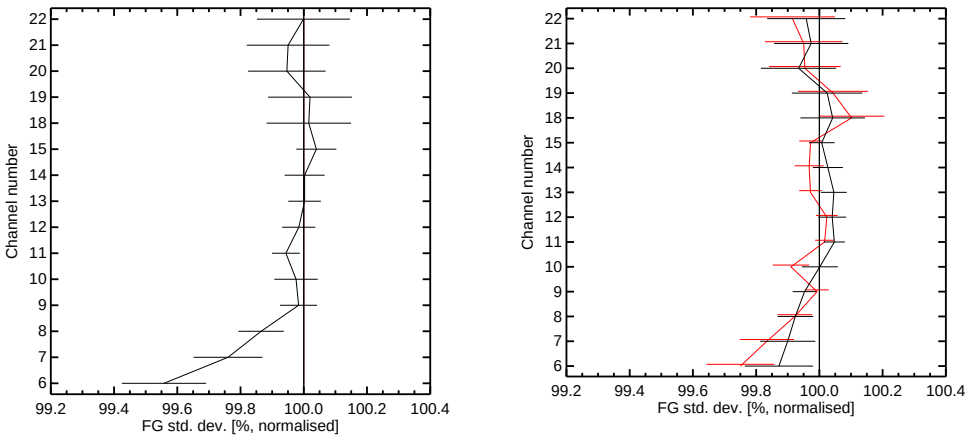

Figure 31: Percentage change in the standard deviation of first guess departures of ATMS for the New observation errors + cloud experiments, normalised to the control. The left shows values for the summer 'New observation errors + cloud 30' experiment and the right shows the winter experiment for 'New observation errors + cloud 30' (red) and 'New observation errors + cloud 45' (black). Note that results are not yet available for the 'New observation errors + cloud 45' summer experiment.

the Southern ocean as shown in figure 33 (bottom) for the 'New observation errors + cloud 45'. This degradation of short-range temperature forecasts could be due to the introduction of warm-biased data for channel 5 over the Southern Hemisphere extra-tropics which affects either the temperature forecasts or the temperature analysis or both. The scatter index check filters for cold-biased (scattering-affected) data but not the warm-biased data of channel 5 (see figure 16). These data have changed the mean analysis, as shown in figure 34, and could also have changed the forecasts and/or the variability of the analysis, either of which would cause the degradation of the forecast scores seen in figure 33 (bottom). If this degradation comes from a more variable analysis this is not necessarily a bad thing. A degradation is not observed in ATMS departure statistics in this area, as shown in figure 35, which indicates that at least the short-range temperature forecasts are not degraded. However since we cannot be sure, it would still be desirable not to have a degradation in the forecast scores and so further investigation is needed. Future work could investigate which channel's data produce the improvements in day 3 geopotential forecast and the degradation in day 1 1000hPa temperature forecasts. It may be that the degradation is due to the introduction of channel 5 data, and the improvements due to the introduction of channels 6 - 8 data. It could also be beneficial to keep a window channel check, at least for channel 5, in order to screen some of the most strongly warm-biased data in the Southern Hemisphere extra-tropics.

4.7 Conclusions

New observation errors were developed for channels 5 - 7 of AMSU-A, containing a noise term, an emissivity term and a cloud term. These new observation errors were tested in a number of assimilation trials, and found to have a neutral impact on forecast scores and fits of observations to 12-hour forecasts using the current operational screening. However the new observations allowed us to test the introduction of more data over high orography, sea-ice and by relaxing the cloud screening, since these new data would be downweighted in the analysis by the new observation errors. The introduction of channel 5 over the Southern Hemisphere sea-ice produced a negative impact on long-range forecast scores, possibly due to introducing data which is biased relative to the model background, and which the system is consequently unable to handle in this part of the globe. The introduction of new data over high orography produced a mainly neutral impact on forecast scores. The relaxing of the cloud screening produced an improvement

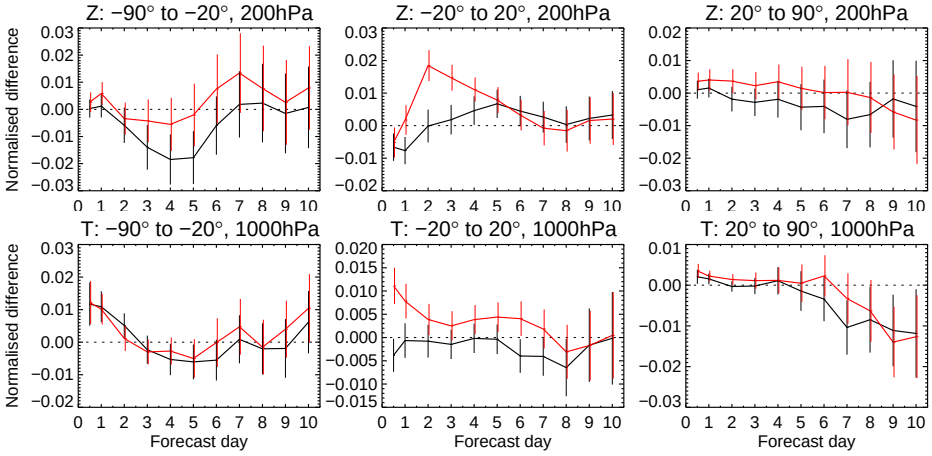

Figure 32: Change in the root mean square forecast minus analysis between the cloud experiments and control. Values are shown as a function of forecast day for the geopotential (top) and temperature (bottom) averaged over all data in the winter period (3 months) for the Southern Hemisphere extratropics, tropics and Northern Hemisphere extratropics (left to right). The black line shows 'New observation errors + cloud 45' - 'control' and the red lines 'New observation errors + cloud 30' - 'control' and negative values show an improvement relative to the control and the error bars indicate a 95 % confidence interval.

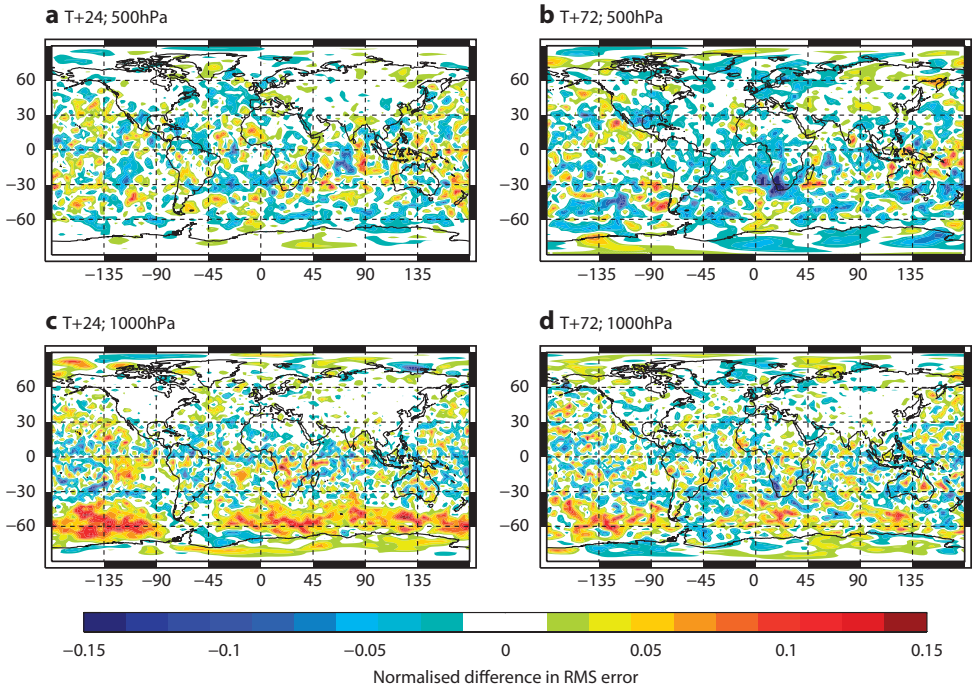

Figure 33: Change in root mean square forecast minus analysis between the 'New observation errors + cloud 45' experiment and control for the winter period (3 months). Values are shown for geopotential (top) and temperature (bottom) on days 1 (left) and 3 (right). Blue areas show an improvement relative to the control experiment and red show a degradation.

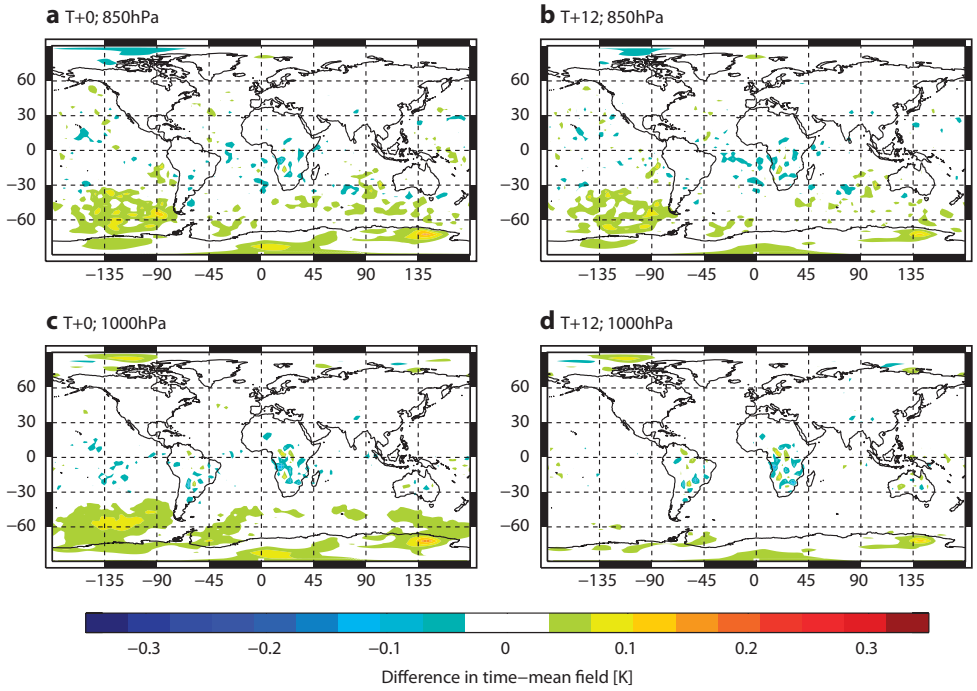

Figure 34: Change in the mean temperature analysis at the start and end of the assimilation window (0h and 12h) at 850hPa (top) and 1000hPa (bottom) between the 'New observation errors + cloud 45' experiment and control.

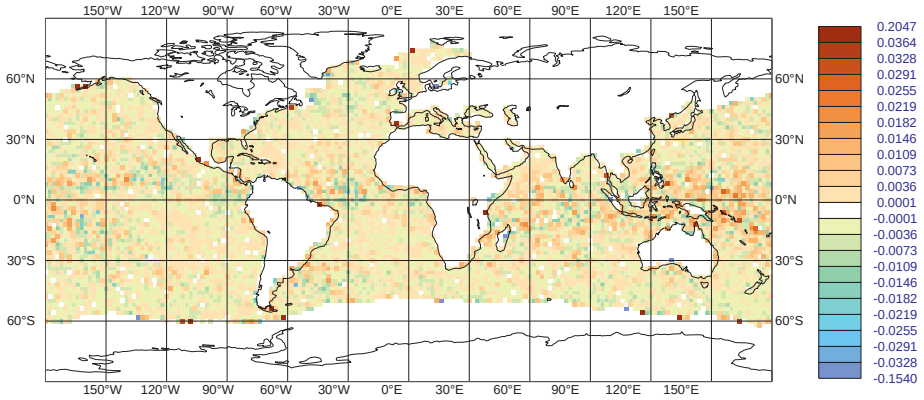

Figure 35: Change in the standard deviation of ATMS background departures between the 'New observation errors + cloud 45' and 'New observation errors' experiments.

in the fit of 12-hour forecasts to ATMS, and an improvement in the forecast scores for geopotential height in the extra-tropics, which was encouraging. There were some negative impacts observed in the short-range temperature forecasts over the southern ocean, which may be due to a degradation in the short-range temperature forecasts or the result of more variability in the analysis due to the introduction of new data.

Future work could test relaxing the cloud screening individually for channels 5 - 8, to investigate which channels are impacting the improved geopotential scores and/or degradations in the short-range temperature scores. The orography screening could also be relaxed further to see whether a positive impact could be obtained.

Acknowledgements

Heather Lawrence's work at ECMWF is funded by the EUMETSAT fellowship programme.

References

[1] N. Bormann and P. Bauer. Estimates of spatial and inter-channel observation error characteristics for current sounder radiances for NWP, part I: Methods and application to ATOVS data. *Q. J. R. Meteorol. Soc.*, 136:1036–1050, 2010.

[2] N. Bormann, A. Fouilloux, and W. Bell. Evaluation and assimilation of ATMS data in the ECMWF system. *J. Geophys. Res.*, 118:12970 – 12980, 2013.

[3] S.J. English. The importance of accurate skin temperature in assimilating radiances from satellite sounding instruments. *IEEE Trans. Geoscience. Rem. Sensing.*, 46:403 – 408, 2008.

[4] A. Geer, P. Bauer, and S. English. Assimilating AMSU-A temperature sounding channels in the presence of cloud and precipitation. *ECMWF Tech. Memo.*, 670, 2012.

[5] N. Grody, J. Zhao, R. Ferraro, F. Weng, and R. Boers. Determination of precipitable water and cloud liquid water over oceans from the NOAA 15 advanced microwave sounding unit. *J. Geophys. Res.*, 106:2943–2953, February 2001.

[6] F. Karbou, E. Grard, and F. Rabier. Microwave land emissivity and skin temperature for amsu-a and -b assimilation over land. *Q.J.Roy.Met.Soc.*, 132:2333–2355, 2006.

[7] F. Karbou, F. Rabier, and C. Prigent. The assimilation of observations from the advanced microwave sounding unit over sea ice in the french global numerical weather prediction system. *Mon. Wea. Rev.*, 142:125 – 140, 2014.

[8] E. Di Tomaso and N. Bormann. Assimilation of ATOVS radiances at ECMWF: third year EUMETSAT fellowship report. *EUMETSAT/ECMWF Fellowship Programme Research Report*, 2013.